An atlas of genetic variation for linking pathogen-induced cellular traits to human disease

Authors:

Liuyang Wang[1], Kelly J. Pittman[1], Jeffrey R. Barker[1], Raul E. Salinas[1], Ian B. Stanaway[2], Robert J. Carroll[3], Tom Balmat[4], Andy Ingham[5], Anusha M. Gopalakrishnan[1], Kyle D. Gibbs[1], Alejandro L. Antonia[1], The eMERGE Network, Joseph Heitman[1,6], Soo Chan Lee[7], Gail P. Jarvick[8], Joshua C. Denny[3], Mark R. DeLong[5], Raphael H. Valdivia[1], David R. Crosslin[2], and Dennis C. Ko[1,6,9*]

Affiliations

[1]Department of Molecular Genetics and Microbiology, School of Medicine, Duke University, Durham, NC 27710

[2]Department of Biomedical Informatics and Department of Medicine, School of Medicine, University of Washington, Seattle, WA 98195

[3]Department of Biomedical Informatics, School of Medicine, Vanderbilt University, Nashville, TN 37212

[4]Social Science Research Institute, Duke University, Durham, NC 27710

[5]Duke Research Computing, Duke University, Durham, NC 27710

[6]Division of Infectious Diseases, Department of Medicine, School of Medicine, Duke University, Durham, NC 27710

[7]South Texas Center for Emerging Infectious Diseases (STCEID), Department of Biology, College of Sciences, The University of Texas at San Antonio, San Antonio, TX 78249

[8]Department of Medicine, Division of Medical Genetics, School of Medicine, University of Washington, Seattle, WA 98195

[9]Lead contact

*To whom correspondence should be addressed: Dennis C. Ko, 0049 CARL Building Box 3053, 213 Research Drive, Durham, NC 27710. 919-684-5834. dennis.ko@duke.edu. @denniskoHiHOST

Summary

Genome-wide association studies (GWAS) have identified thousands of genetic variants associated with disease. To facilitate moving from associations to disease mechanisms, we leveraged the role of pathogens in shaping human evolution with the Hi-HOST Phenome Project (H2P2): a catalog of cellular GWAS comprised of 79 phenotypes in response to 8 pathogens in 528 lymphoblastoid cell lines. Seventeen loci surpass genome-wide significance ($p<5x10^{-8}$) for phenotypes ranging from pathogen replication to cytokine production. Combining H2P2 with clinical association data from the eMERGE Network and experimental validation revealed evidence for mechanisms of action and connections with diseases. We identified a SNP near *CXCL10* as a cis-cytokine-QTL and a new risk factor for inflammatory bowel disease. A SNP in *ZBTB20* demonstrated pleiotropy, partially mediated through NFκB signaling, and was associated with viral hepatitis. Data are available in an H2P2 web portal to facilitate further interpreting human genome variation through the lens of cell biology.

Keywords: genome-wide association study, lymphoblastoid cell line, immune quantitative trait locus, heritability, pleiotropy, phewas, electronic medical record, CXCL10, ZBTB20, eldelumab

Introduction

The human genome has been shaped by migration, drift, admixture, and natural selection (Cavalli-Sforza et al., 1994; Li et al., 2008; Pickrell and Reich, 2014). One of the strongest driving forces in natural selection has been pathogens (Fumagalli et al., 2011; Pittman et al., 2016), as first exemplified with A. C. Allison's demonstration that sickle cell allele (rs334) conferred resistance to malaria (Allison, 1954). Red blood cells from individuals with this allele are resistant to *Plasmodium* infection (Friedman, 1978). Similarly, human resistance to HIV infections afforded by the *CCR5Δ32* allele can also be seen at the level of individual T cells (Dean et al., 1996; Liu et al., 1996; Samson et al., 1996). Therefore, identification and characterization of human genetic differences that impact cellular traits can help mechanistically link human genetic variation to disease susceptibility.

Previous studies have examined the genetic basis of molecular traits in human populations. Expression quantitative trait loci (eQTL) studies in lymphoblastoid cell lines (LCLs) defined abundant associations between human SNPs and expression levels of nearby genes (Stranger et al., 2012; Stranger et al., 2007). LCLs are EBV-transformed B cells that are highly similar to antigen-activated primary B cells (Cahir-McFarland et al., 2004). LCLs serve as a standardized resource for functional human genetic variation studies, as they have been densely genotyped by the International HapMap Project (Consortium, 2005; International HapMap et al., 2010) and the 1000 Genomes Project (Consortium, 2010). As eQTLs are often shared across tissues (e.g. 88% of cis-eQTLs are shared among LCLs, fibroblasts, and primary T cells (Flutre et al., 2013)), LCL eQTL studies have led to important insights not only in immunity-related diseases but also for disorders such as autism where B cells are not believed to be primary

drivers of disease (Nica and Dermitzakis, 2013). Thus, LCLs can serve as a powerful platform to identify and characterize the role of human genetic variation in a variety of diseases.

Using LCLs, we developed Hi-HOST (High-throughput Human in vitrO Susceptibility Testing) as a platform for identifying human genetic differences in pathogen-induced cellular traits that provides a cell biological link between eQTL studies and GWAS of human disease (Ko et al., 2009; Ko and Urban, 2013). Hi-HOST uses live pathogens to examine variation in innate immune recognition, but also in cell biological and signaling processes that can be quantified as phenotypes for genome-wide association. This work therefore builds on a long tradition of using cellular microbiology to elucidate basic cell biology (Cossart et al., 1996) and expands that utility to interpret the human genome. Using Hi-HOST, we leveraged LCL responses to *Salmonella enterica* to demonstrate that genetic variation in the methionine salvage pathway regulates pyroptosis, as well as human susceptibility to sepsis (Ko et al., 2012; Wang et al., 2017). Similarly, we recently reported that a genetic variant in *VAC14* is associated with both increased *S.* Typhi invasion into LCLs and risk of typhoid fever in a Vietnamese population (Alvarez et al., 2017).

Here, we present the Hi-HOST Phenome Project (H2P2) to globally explore the genetic basis of cellular outcomes in response to infectious agents. Using 7 microbes and 1 bacterial toxin, we carried out GWAS of 79 host-pathogen phenotypes that serve as cellular readouts for processes such as endocytosis, endosomal trafficking, signal transduction, cell death, and transcriptional regulation. We identified 17 loci that reached the generally accepted threshold for genome-wide significance ($p<5x10^{-8}$). We integrated H2P2 data with experimental validation and disease association data from the eMERGE Network PheWAS pipeline (Denny et al., 2013) to define new functions for genes in disease and provide new clues to disease pathophysiology.

Results

Phenotypic variation in H2P2 traits reveals biologically meaningful clusters

We measured variation in cellular traits in 528 LCLs stimulated with 7 different microbes and 1 bacterial toxin (Figure 1A). These LCLs have been genotyped (Consortium, 2010) and consist of 4 human populations: ESN (Esan in Nigeria), GWD (Gambians in Western Divisions in the Gambia), IBS (Iberian Population in Spain), and KHV (Kinh in Ho Chi Minh City, Vietnam). The LCLs used in this study were all from parent-offspring trios, allowing for heritability estimation by parent-offspring regression and for carrying out combined GWAS analysis with protection from stratification through family-based association methods (Purcell et al., 2007; Purcell et al., 2005).

The microbes and toxin we selected affect billions of people worldwide. Non-typhoidal *Salmonella* infections caused 150 million diarrheal illnesses (gastroenteritis) and 0.6 million cases of invasive enteric disease (bacteremia) in 2010 (Kirk et al., 2015; Majowicz et al., 2010). Approximately 20 million cases of typhoid fever are caused by *Salmonella enterica* serovar Typhi (*S.* Typhi) every year (Dougan and Baker, 2014). *Chlamydia trachomatis*, the most common bacterial sexually transmitted infection in the world, causes 100 million cases of genital tract infection every year (Newman et al., 2015), and 1.3 million individuals are blind due to ocular infection with *C. trachomatis* (Burton and Mabey, 2009). *Staphylococcus aureus* is a common cause of skin and soft tissue infections, bacteremia, and infective endocarditis, and its alpha toxin, which is utilized in H2P2, is a key virulence determinant (Tong et al., 2015). *Candida albicans* and related fungal species are a frequent cause of genitourinary tract infection that can cause more severe disease in immunocompromised individuals and are the fifth most common cause of hospital-associated infections (Yapar, 2014). *Mucor circinelloides* is another

fungal species that causes severe infections, mucormycosis, in immunocompromised individuals (reviewed in (Mendoza et al., 2014)) and has also recently been connected to food-borne infections (Lee et al., 2014). Finally, over 6 billion people in the world have been infected with the protozoal pathogen *Toxoplasma gondii*, which can be fatal in infants and immunocompromised individuals (Furtado et al., 2011). Thus the microbes and toxin used in H2P2 are important causes of human disease.

Beyond their role in human disease, the pathogens selected also exploit a wide range of host cellular processes to either kill the host cell or to create replicative niches within them. *C. trachomatis, S. enterica* serovar Typhi, serovar Typhimurium (wildtype and Δ*sifA* mutant, which escapes from the pathogen-containing vacuole at a greater rate into the host-cell cytosol (Beuzon et al., 2000)), and *T. gondii* are intracellular pathogens that employ diverse lifestyles, evading killing mechanisms and relying on host cell biology to provide nutrients. These microbes were engineered to express the green-fluorescent protein (GFP) to allow quantitation of pathogen invasion, survival and replication, intercellular spread, and concurrent measurement of cell death by flow cytometry. Cell death was also measured as the readout for *Staphylococcus aureus* alpha toxin, a pore-forming toxin that causes cell lysis (Tong et al., 2015). Microbes were also tested for induction or suppression of cytokines in infected LCLs, providing multiple readouts of host-cell signaling pathways. *S.* Typhimurium and *C. trachomatis*-infected cells were measured for 3 and 17 cytokines, respectively. The fungal pathogens *M. circinelloides* and *C. albicans* were included for their ability to induce FGF-2 in LCLs (Lee et al., 2015). Definitions for all 79 phenotypes as well as histograms for phenotypes are provided in the supplemental data (Table S1 and Figure S1). Importantly, 76 of 79 H2P2 phenotypes showed significant experimental repeatability based on measurements on LCLs from three different passages (Figure S2).

Hierarchical clustering of traits based on inter-individual variation confirmed the robustness of our measurements (Figure 1B). Levels of three cytokines (CXCL10 (IP-10), IL-10, and MDC) measured in uninfected cells with two different methods (ELISA at 24hrs post-plating and Luminex at 70hrs) showed strong correlation (R = 0.78 for CXCL10, R= 0.46 for IL-10, R=0.90 for MDC; Spearman correlation). The clustering of responses to *Salmonella* infection is consistent with previous findings: *S.* Typhimurium, Typhi, and Typhimurium Δ*sifA* cluster for the phenotype of invasion, as all utilize a similar type-3 secretion system for entry (Collazo and Galan, 1997) (correlation to *S.* Typhimurium, R=0.69 for *S.* Typhi and R=0.90 for *S.* Typhimurium Δ*sifA*). In contrast, the correlation is weaker for intracellular survival and replication phenotypes (correlation to *S.* Typhimurium replication from 3.5 hrs to 24 hrs, R=0.36 for *S.* Typhi and R=0.34 for *S.* Typhimurium Δ*sifA*), reflecting the different replications niches for Δ*sifA* (host cell cytoplasm) and wild-type Typhimurium (membrane bound vacuole) (Beuzon et al., 2000) or the use of a different repertoire of effectors by *S.* Typhi (Parkhill et al., 2001). Thus, clustering based on phenotypic diversity verified the reliability of measurements and confirmed biological relatedness established by previous work from multiple groups.

H2P2 traits are heritable based on parent-offspring regression and SNP-based heritability

If genetic differences regulate variation in cellular phenotypes, then the additive contributions of these differences to phenotypic variance can be estimated. We measured narrow-sense heritability (h^2) with two independent and complementary methods: parent-offspring regression and SNP-based h^2. Heritability based on parent-offspring regression is estimated as the slope of the regression line for offspring phenotypes vs. mid-parent phenotypes (Falconer and Mackay, 1996). We observed h^2 estimates from -0.06 to 0.85 (average h^2=0.33), with the largest h^2 observed for *S.* Typhimurium-induced levels of IL-10 (h^2=0.85±0.19,

$p=3.5x10^{-15}$) (Figure 1C; Figure S3; Table S2). The majority (64/79) of phenotypes showed significantly non-zero h^2 by this method ($p<0.05$). In contrast, SNP-based h^2, as implemented in the GCTA software package (Yang et al., 2011) with the Zaitlen modification for related individuals (Zaitlen et al., 2013), calculates the proportion of variance that can be explained by all genotyped SNPs. With this method, we observed pedigree h^2 ranging from 0.04 to 0.76 (average $h^2=0.36$), and SNP-based h^2 ranging from 0.02 to 0.66 (average $h^2=0.19$) (Figure 1C; Table S2).

We observed high correlation between h^2 estimated using the two different methods ($R=0.58$; $p=2.9x10^{-8}$; Figure 1D). The strong correlation between the two estimates of h^2, based on distinct statistical frameworks, provides additional evidence that LCLs provide a robust system to identify human SNPs that contribute to the heritability of cellular phenotypes.

H2P2 reveals 17 genome-wide significant associations and enrichment for genic SNPs and regions of active chromatin

We performed a family-based GWAS in PLINK (Purcell et al., 2007; Purcell et al., 2005) on 79 traits for 528 LCLs using dense genotyping information (15.5 million SNPs after imputation; see Methods). Across 79 traits, we observed 17 loci that reached a genome-wide significance threshold of $p<5x10^{-8}$ (Figure 2A; Table 1; Figure S4). H2P2 demonstrated enrichment of associated SNPs for functional genome annotations. We used the GARFIELD package to calculate and visualize fold-enrichment of SNPs associated in H2P2 at variable p-value thresholds with different genomic features (Iotchkova et al., 2016). In regards to SNP location, the greatest enrichment was observed for exonic SNPs (Figure 2B). The fold-enrichment was highest at the most stringent p-value threshold ($p<1x10^{-8}$) for H2P2 traits (9.2-fold enrichment; $p=0.10$ by Fisher's exact test) and was statistically significant when using a

$p<5x10^{-8}$ threshold for H2P2 traits (3.9 fold-enrichment; p=0.047). In contrast, there was depletion for intergenic SNPs at the $p<5x10^{-8}$ threshold (0.66 fold-enrichment). H2P2-associated SNPs showed even greater enrichment for regions of active chromatin as annotated by DNase hypersensitivity peaks from the ENCODE project (Consortium et al., 2012) (Figure 2C). Consistent with H2P2 being conducted in LCLs, the 2nd greatest enrichment was observed for DNAase hypersensitivity peaks measured in the LCL GM06990 out of 424 cell types measured (at $p<5x10^{-8}$, 5.7 fold-enrichment; $p=3.8x10^{-3}$). Even stronger enrichment was noted at this threshold for human Th2 cells (7.3 fold-enrichment; $p=3.5x10^{-4}$), and enrichment was observed for cells derived from most tissues (Figure 2C), consistent with LCLs being a relevant model for genetic analysis for multiple human cell types.

A large-effect cis-regulatory variant regulates CXCL10 levels

The strongest association in the H2P2 dataset was observed for rs2869462 with levels of the chemokine CXCL10 (also known as IP-10) following *Chlamydia* infection ($p=2x10^{-9}$; Figure 2D, E). This SNP is located 7.5kb 3' of the *CXCL10* coding sequence (Figure 2D) in a region that also encodes for two related chemokines, CXCL9 and CXCL11. These chemokines bind to CXC-chemokine receptor 3 (CXCR3), a G-protein coupled receptor that mediates inflammation by coordinating T-helper 1 (Th1) recruitment and activating effector cells during infection and autoimmunity (reviewed in (Groom and Luster, 2011)). Many cell types produce CXCL10 during infection, including activated B cells (Hennig et al., 2014; Hoff et al., 2015; Kato et al., 2004; Vollmer et al., 2004). Notably, the effect of this SNP is large: rs2869462 accounts for 13.7% of the variance in CXCL10 protein levels.

Although rs2869462 was identified using genome-wide association of all 528 LCLs in our dataset, there were large differences in allele frequencies among the populations. The derived

allele of rs2869462 (G) is present at the highest frequencies in Europe (28% in IBS) and Asia (28% in KHV) and is substantially lower in Africa (1.5% in ESN, 1% in GWD; Figure 2F). Strikingly, all populations demonstrated the same directionality of effect for the rs2869462 allele on CXCL10 levels (C > G) (Figure 2G).

SNPs lead to pleiotropic effects on multiple pathogen-induced traits

Different pathogens can target common signaling pathways to establish an intracellular niche or to modulate immune responses. Therefore, we examined whether genome-wide significant hits were associated with just one trait or if they were associated with multiple traits, using either a threshold of $p<0.05$ or with Bonferroni multiple-test correction ($p<6.3x10^{-4}$). All of the 17 genome-wide significant hits were associated with at least 4 H2P2 traits with the $p<0.05$ threshold (Figure 3A). However, several phenotypes are closely related and therefore these cross-phenotype associations do not reflect true pleiotropy, multiple unrelated effects due to the same gene (Solovieff et al., 2013). For example, rs2869462 had 5 cross-phenotype associations but 4 of these traits are based on CXCL10 levels (*Chlamydia*-infected levels, uninfected by Luminex measurement at 70 hrs, uninfected by ELISA at 24 hrs, and *Salmonella* Typhimurium-infected levels) (Figure 3B). Beyond the existence of pleiotropy, the pattern of which traits shared genetic associations provided additional insight (Figure 3C). A circle plot of cross-phenotype associations showed most cross-phenotype associations in H2P2 connect invasion, establishment of an intracellular niche, and intercellular spread. Traits that had high phenotypic correlation (Figure 1B) were more likely to have cross-phenotypic associations as expected (Figure 3D).

The greatest number of associated traits at $p<0.05$ occurred for rs953897, a SNP in the gene encoding the transcriptional repressor ZBTB20. Based on GTEx data, rs953897 is

235 associated with *ZBTB20-AS1* transcript abundance ($p=6.9x10^{-8}$) (Consortium, 2015). While rs953897 is most strongly associated with high *C. trachomatis* burden at 46 hrs ($p = 1.3x10^{-8}$), this SNP was associated with 20 H2P2 traits ($p<0.05$) and 5 traits using a multiple-test corrected threshold of $p<6.3x10^{-4}$. A QQ plot comparing p-values for all traits for rs953897 confirmed the high degree of pleiotropy for this SNP, demonstrating strong deviation from neutrality towards 240 lower p-values (Figure 3D). These associations even included other pathogens and biological processes, as the third most strongly associated trait was *S.* Typhimurium-induced pyroptosis ($p=7.5x10^{-5}$; Figure 3D). Overall, out findings indicate that genetic variation in *ZBTB20* is linked to pleiotropic effects on multiple host-pathogen traits.

Genetic variants impacting ZBTB20 expression affect the outcome of Chlamydia and Salmonella 245 *infections*

The T allele of rs953897 was associated with both higher levels of *Chlamydia* replication ($p=1.3x10^{-8}$; Figure 4A) and *Salmonella*-induced pyroptosis ($p=7.5x10^{-5}$; Figure 4B). Reduction of *ZBTB20* expression by RNAi increased *Chlamydia* replication and pyroptosis, mimicking the effect of the T allele (Figure 4C, D). RNAi-mediated depletion of ZBTB20 also indicated that 250 some phenotypes that did not reach statistically significant associations with rs953897 after multiple-test correction were nonetheless mediated by ZBT20. Specifically, expression of IL-6 after infection with *Chlamydia* ($p=0.03$), was *reduced* after *ZTB20* RNAi treatment, again mimicking the effect of the T allele (Figure 4E). The effect of ZBT20 depletion on IL-6 expression is not the result of decreased bacterial burden since *Chlamydia* replication was 255 enhanced under these conditions. Thus, the association data and functional validation point to a role for ZBTB20 in the regulation of multiple infection-related phenotypes.

ZBTB20 has been characterized as a transcriptional repressor during prenatal development in the liver and the brain (Mitchelmore et al., 2002; Nielsen et al., 2007; Xie et al., 2008). Rare protein-coding mutations in *ZBTB20* are responsible for Primrose syndrome, which has features as disparate as mental retardation, ossified external ears, and distal muscle wasting (Cordeddu et al., 2014). We hypothesized that one ZBTB20 target gene could regulate a pathway that impacted multiple biological processes related to pathogen immunity. An attractive target, IκB (*NFKBIA*), the canonical suppressor of NFκB signaling, is subject to ZBTB20 transcriptional repression (Liu et al., 2013). Reduction of ZBTB20 expression in LCLs by RNAi causes increased expression of IκB (Figure 4F). An increase of IκB should cause inhibition of NFκB signaling, resulting in increased *Chlamydia* replication but decreased expression of pro-inflammatory cytokines including IL-6. Consistent with this prediction, depletion of IκB by RNAi decreased *Chlamydia* replication and increased IL-6 production (Figure 4C, E). In contrast, depletion of IκB did not impact *Salmonella*-induced pyroptosis, indicating an IκB-independent mechanism (Figure 4D). These observations point to multiple roles for ZBTB20 in regulating cellular functions during infection, both through suppression of regulators of signaling pathways, such as NFκB (Figure 4J), but also through regulation of other unidentified targets.

SNPs linked to CXCL10 expression are also associated with infection, inflammatory sequelae, and IBD

We determined if SNPs associated with cellular traits in H2P2 were associated with human disease. Examination of the NHGRI-EBI GWAS catalog (Welter et al., 2014) did not reveal any associations with rs2869462 or any other SNPs in *CXCL10*. We next performed a PubMed search for *CXCL10* SNP association in candidate gene studies in the context of infectious diseases. rs2869462 has not been previously examined, but a SNP in modest LD

(rs3921, r^2=0.3 in Europeans in 1000 Genomes) that had been reported in five previous studies of infectious disease showed association with *Chlamydia*-infected CXCL10 levels ($p=6.4x10^{-4}$) in our dataset (Fisher et al., 2017; Mezger et al., 2008; Nogueira et al., 2012; Pineda-Tenor et al., 2015; Pineda-Tenor et al., 2014). The rs3921 allele associated with higher levels of CXCL10 in H2P2 (C), was also associated with protection against invasive aspergillosis (Fisher et al., 2017; Mezger et al., 2008) and greater odds of sustained virologic response in HIV/HCV co-infected individuals (Pineda-Tenor et al., 2014) (Figure 5A). The high CXCL10 allele also leads to increased risk of liver fibrosis in HIV/HCV co-infected individuals (Pineda-Tenor et al., 2015) and severe cardiomyopathy in Chagas disease (Nogueira et al., 2012), suggesting that increased inflammatory sequelae may be an unintended consequence of the high CXCL10 allele.

Consistent with the rs2869462 C allele being associated with increased inflammation, we discovered that this allele is a previously unrecognized inflammatory bowel disease (IBD) risk allele. Recently, CXCL10 inhibitory antibodies have undergone phase II clinical trials for both sub-types of IBD, Crohn's disease (CD) and ulcerative colitis (UC) (Sandborn et al., 2016; Sandborn et al., 2017), based on evidence from animal models (Hyun et al., 2005; Sasaki et al., 2002; Singh et al., 2003) and of elevated CXCL10 in patients with CD (Ostvik et al., 2013) and UC (Uguccioni et al., 1999). Comparison to publicly available GWAS summary statistics from the IBD Genetics Consortium meta-analysis of 12882 IBD cases and 21770 controls (Liu et al., 2015) demonstrated that rs2869462 is associated with IBD ($p=1.7x10^{-4}$; OR=1.08), as well as with CD ($p=1.9x10^{-3}$; OR=1.09) and UC subtypes (p=0.016; OR=1.06) (Figure 5B; 5C). The cases in the two subtypes are exclusive of one another and therefore demonstrate an association of rs2869462 with two different cohorts of IBD cases (though most controls are shared).

Furthermore, the direction of association is consistent with high levels of CXCL10 (the C allele) being associated with greater risk of IBD.

We independently tested for this association using electronic medical record (EMR) data from the eMERGE Network (McCarty et al., 2011). The eMERGE dataset holds genotype-phenotype correlations of >80,000 individuals (with PCA-correction for population stratification) with phenotypes assigned based on ICD-9 patient billing codes (Denny et al., 2013). While there is no code for IBD or Crohn's disease *per se*, there is a code for "ulcerative colitis (chronic)." Though power is limited with only 743 cases (and 47093 controls), rs2869462 was associated with this phenotype in the predicted direction (p=0.02; OR=1.16, C allele) (Figure 5C). Therefore by first identifying a SNP as associated with CXCL10 levels following an LCL model of *C. trachomatis* infection, we have discovered and replicated a new IBD risk allele (Figure 5D).

H2P2 SNPs are associated with disease in PheWAS of electronic medical record traits

Next, we systematically generated hypotheses regarding the effects of the H2P2 genome-wide significant hits on human disease by employing a PheWAS (phenome-wide association study) approach, looking for FDR<=0.3 associations across a large set (1865) of clinical measurements and diseases cataloged in eMERGE (Denny et al., 2013). We found 13 of 16 H2P2 genome-wide significant hits surpassed the 0.3 FDR threshold with at least 1 EMR phenotype (Figure 6A; Table S3; 1 H2P2 SNP was not in the eMERGE dataset and had no good proxy based on LD). Thirty associations with eMERGE traits were detected and eleven of these involved infectious disease or clinical immune-related traits.

While rs2869462 replicated the association with UC as described above, this SNP showed an association by PheWAS with "keloid scar" ($p=1x10^{-4}$; FDR=0.16; OR=0.62, C allele; Figure 6B). Keloids are abnormal fibrotic skin lesions that are believed to be influenced by genetic susceptibility (Shih and Bayat, 2010). Notably, a Th1 response has antifibrotic activity (Wynn and Ramalingam, 2012), consistent with the protective effect of high CXCL10 suggested by this association. Another SNP (rs4949082) was associated with CXCL10 levels following *Salmonella* Typhimurium infection in H2P2 ($p=3.7x10^{-8}$). This SNP shows an association with "deficiency of humoral immunity" ($p=6.4x10^{-5}$; FDR=0.11; OR=1.25; Figure 6C), which is consistent with CXCL10's role as a key determinant of Th1 (cellular) vs. Th2 (humoral) immune response. CXCL10 also regulates the differentiation of plasma cells, which produce high levels of antibody (Xu et al., 2012).

Similarly, rs953897 in *ZBTB20* was associated with viral hepatitis ($p=1.88x10^{-4}$; FDR=0.26; OR=1.18). Most of the 1679 viral hepatitis cases are due to hepatitis C virus. The allele associated with higher *Chlamydia* replication, and likely less NFκB activation (T), was associated with *lower* risk of viral hepatitis. This is consistent with a recent report indicating that NFκB activation promotes viral entry into hepatocytes through disruption of tight junctions (Fletcher et al., 2017). Our data indicate that ZBTB20 may regulate this signaling pathway during viral infection in humans.

The SNP that had the greatest number of PheWAS associations was rs7566597. This SNP, associated with the H2P2 phenotype of *Chlamydia*-infected levels of the chemokine MIP-1β (macrophage inflammatory protein-1beta; CCL4), was associated with six clinical traits. One of the most significant associations ($p =1.2x10^{-4}$; FDR=0.07; OR=1.33) was observed with otorrhea (Figure 6D). Otorrhea is ear drainage most commonly caused by an ear infection.

Notably, MIP-1β is elevated in fluid from patients with middle ear infections (Kaur et al., 2015), mice with genetic predisposition to middle ear infections (Han et al., 2012), and primary middle ear epithelial cultures infected *in vitro* with either influenza or *Streptococcus pneumoniae* (Tong et al., 2003). The directionality of this association (G allele associated with both higher MIP-1β levels and increased risk of otorrhea), and the fact that genotype is fixed prior to disease, lead to the hypothesis that the rs7566597 G allele causes higher levels of MIP-1β to increase risk of otorrhea.

Discussion

With H2P2, we have coupled the ability of pathogens to influence genetic diversity in human populations to their use as cellular probes to elucidate mechanisms of disease. This cellular GWAS approach provides: 1) biomolecules and proteins that could serve as possible biomarkers and therapeutic targets and 2) a cellular model to validate and dissect mechanisms of how the genetic variant regulates the cell biological process now connected to disease. We have developed an H2P2 database and web interface to allow for exploration of this rich dataset by the research community (http://h2p2.oit.duke.edu).

Cellular GWAS studies have also been performed on inter-individual variation in levels of immune cell subtypes, cell surface protein expression, and cytokine levels (Li et al., 2016; Orru et al., 2013; Roederer et al., 2015). However, Hi-HOST is unique in using live pathogens to induce complex cellular phenotypes, such as cell death and invasion, providing surrogate phenotypes that are intermediate between molecular phenotypes of gene/protein expression and human population studies of disease. Additionally, H2P2 utilizes cells derived from multiple human populations. Notably, allele frequencies for rs2869462 and rs953897 vary greatly across the globe. These differences may play an important role in susceptibility of different populations

in cellular responses and disease. Finally, our use of parent-offspring trios allowed us to make estimates of h^2 through both parent-offspring regression and SNP-based methods.

Our h^2 estimates are consistent with a large fraction of variation in cellular responses as being genetically determined. For parent-offspring regression 64 of 79 traits had significantly non-zero h^2 ($p<0.05$). While relatively small sample size led to large standard errors for SNP-based estimates of h^2, the two estimates correlated quite strongly ($r=0.58$; $p=2.9x10^{-8}$). Our estimates of h^2 are similar to other reports for immune-related traits. Orru *et al.* examined levels of 95 immune cell types and found a mean h^2 of 41% (range 3-87%) (Orru et al., 2013). Our estimates of h^2 for cytokine levels as well as for more complex host-pathogen phenotypes such as *Chlamydia* intracellular replication (46hr % high GFP; 33% by parent-offspring regression and 20% by SNP-based heritability) are consistent with a strong genetic basic for variation in immune cell traits and host-pathogen interactions, though environment also has a large effect. Furthermore, our ability to identify SNPs strongly associated with these traits that can explain a sizable portion of the h^2 further confirms the importance of common SNPs in contributing to the h^2 of molecular and cellular pathogen-induced traits.

Integrating H2P2 with human genetic association data from published studies and the eMERGE Network revealed how genetic variants impacting cellular traits also influenced human disease. For rs2869462, we found that this SNP associated with CXCL10 levels is also a previously unrecognized risk factor for IBD. While over a hundred IBD risk alleles have been identified (Liu et al., 2015), the fact rs2869462 was associated with levels of CXCL10 in H2P2 may make genotyping of this SNP clinically actionable if coupled to anti-CXCL10 therapy. While anti-CXCL10 demonstrated some benefit in phase 2 trials, neither study met statistical significance for its primary endpoint (Sandborn et al., 2016; Sandborn et al., 2017). We

hypothesize that rs2869462 genotype might be a predictive biomarker for identifying the genetic subtype of patients who show the greatest benefit. This example, spanning molecular phenotype, human disease, and clinical utility serves as a template for how we envision the H2P2 web portal being used to make similar discoveries.

For both *CXCL10*, *ZBTB20*, and other genes implicated by H2P2 there are numerous associations that do not reach genome-wide significance but are undoubtedly true-positives based on highly related phenotypes or experimental evidence. Indeed, our lab has previously pursued non-genome-wide significant hits revealed by Hi-HOST, resulting in a new metabolite biomarker for sepsis (Wang et al., 2017) and a new potential therapeutic strategy for typhoid fever (Alvarez et al., 2017). However, to fully illuminate how genetic variation contributes to the pathophysiology of disease will require the engagement of the research community with the H2P2 web portal and other similar datasets. These users, already experts on particular genes and/or cellular pathways, would be well-equipped to then validate and discover the mechanisms underlying these associations. Thus, H2P2 provides a hypothesis-generating engine for identifying new biomarkers and therapeutic strategies. Future studies will expand the panel of stimuli and the cell types used to create a more complete picture of how cellular traits impact human health and disease, an important step towards a future of more personalized care.

Author Contributions

All authors critically reviewed the manuscript and contributed input to the final submission. DCK, LW, KJP, ALA, IBS, TB, RHV, and DRC wrote the manuscript. DCK, LW, KJP, ALA, JH, SCL, RHV, and DRC contributed to strategy and project planning. KJP, DCK, JRB, RES, AMG, KDG, YC, and SCL carried out experiments and analysis. LW, IBS, RJC, tEM, JCD, DRC, and DCK planned and carried out computational analysis and provided datasets. TB, AI, LW, MRD, and DCK designed and implemented the H2P2 database and web portal.

Competing interests: Duke University has submitted a provisional patent application ("A Companion Diagnostic for IBD Therapy") on behalf of DCK, LW, and ALA.

Acknowledgments: Funding: LW, KJP, RES, KDG, ALA, YC, and DCK were supported by NIH R01AI118903. LW, KJP, JRB, RES, AMG, RHV, and DCK were supported by the Ecopathogenomics of Sexually Transmitted Infections (EPSTI) Cooperative Research Center (NIH U19AI084044). DCK was also supported by a Duke University Whitehead Scholarship, the Butler Pioneer Award, and a Duke MGM Pilot Award. IBS, RJC, JCD, and DRC were supported by eMERGE Network (Phase III). This phase of the eMERGE Network was initiated and funded by the NHGRI through the following grants: U01HG8657 (Group Health Cooperative/University of Washington); U01HG8685 (Brigham and Women's Hospital); U01HG8672 (Vanderbilt University Medical Center); U01HG8666 (Cincinnati Children's Hospital Medical Center); U01HG6379 (Mayo Clinic); U01HG8679 (Geisinger Clinic); U01HG8680 (Columbia University Health Sciences); U01HG8684 (Children's Hospital of Philadelphia); U01HG8673 (Northwestern University); U01HG8701 (Vanderbilt University Medical Center serving as the Coordinating Center); U01HG8676 (Partners Healthcare/Broad Institute); and U01HG8664 (Baylor College of Medicine). U01HG004438 (CIDR) and

U01HG004424 (the Broad Institute) served as eMERGE Genotyping Centers. SCL was supported by NIH/NIAID R03 AI11917 and UTSA Research funds. JH was supported by NIH/NIAID R37 MERIT Award AI39115-20, NIH/NIAID R01 AI50113-13, and an award from Astellas. TB, AI, and MRD were supported by Duke Research Computing. We thank Dr. Yanlu Cao for performing FGF-2 ELISAs. We thank Luke C. Glover for help in plotting association data. We thank Dr. Gregory D. Sempowski and the Duke Immune Reconstitution & Biomarker Analysis Shared Resource in performing pilot Luminex measurements. We thank Drs. Shelton Bradrick, David Tobin, Ana-Maria Xet-Mull, Andrew Alspaugh, and Jennifer L. Trenor for pilot studies in characterizing infection into LCLs. DNA image from Figure 1 is from the National Human Genome Research Institute Image Gallery. The content of this manuscript is solely the responsibility of the authors and does not necessarily represent the official views of the National Institutes of Health or other funding sources.

References

Allison, A.C. (1954). Protection afforded by sickle-cell trait against subtertian malareal infection. Br Med J *1*, 290-294.

Alvarez, M.I., Glover, L.C., Luo, P., Wang, L., Theusch, E., Oehlers, S.H., Walton, E.M., Tram, T.T.B., Kuang, Y.L., Rotter, J.I., *et al.* (2017). Human genetic variation in VAC14 regulates Salmonella invasion and typhoid fever through modulation of cholesterol. Proc Natl Acad Sci U S A.

Bastidas, R.J., and Valdivia, R.H. (2016). Emancipating Chlamydia: Advances in the Genetic Manipulation of a Recalcitrant Intracellular Pathogen. Microbiol Mol Biol Rev *80*, 411-427.

Beuzon, C.R., Meresse, S., Unsworth, K.E., Ruiz-Albert, J., Garvis, S., Waterman, S.R., Ryder, T.A., Boucrot, E., and Holden, D.W. (2000). Salmonella maintains the integrity of its intracellular vacuole through the action of SifA. EMBO J *19*, 3235-3249.

Burton, M.J., and Mabey, D.C. (2009). The global burden of trachoma: a review. PLoS Negl Trop Dis *3*, e460.

Cahir-McFarland, E.D., Carter, K., Rosenwald, A., Giltnane, J.M., Henrickson, S.E., Staudt, L.M., and Kieff, E. (2004). Role of NF-kappa B in cell survival and transcription of latent membrane protein 1-expressing or Epstein-Barr virus latency III-infected cells. Journal of virology *78*, 4108-4119.

Carroll, R.J., Bastarache, L., and Denny, J.C. (2014). R PheWAS: data analysis and plotting tools for phenome-wide association studies in the R environment. Bioinformatics *30*, 2375-2376.

Cavalli-Sforza, L.L., Menozzi, P., and Piazza, A. (1994). The history and geography of human genes (Princeton, N.J.: Princeton University Press).

Chang, C.C., Chow, C.C., Tellier, L.C., Vattikuti, S., Purcell, S.M., and Lee, J.J. (2015). Second-generation PLINK: rising to the challenge of larger and richer datasets. Gigascience *4*, 7.

Collazo, C.M., and Galan, J.E. (1997). The invasion-associated type-III protein secretion system in Salmonella - A review. Gene *192*, 51-59.

Consortium, E.P., Dunham, I., Kundaje, A., Aldred, S.F., Collins, P.J., Davis, C.A., Doyle, F., Epstein, C.B., Frietze, S., Harrow, J., *et al.* (2012). An integrated encyclopedia of DNA elements in the human genome. Nature *489*, 57-74.

Consortium, G.P. (2010). A map of human genome variation from population-scale sequencing. Nature *467*, 1061-1073.

Consortium, G.T. (2015). Human genomics. The Genotype-Tissue Expression (GTEx) pilot analysis: multitissue gene regulation in humans. Science *348*, 648-660.

Consortium, I.H. (2005). A haplotype map of the human genome. Nature *437*, 1299-1320.

Cordeddu, V., Redeker, B., Stellacci, E., Jongejan, A., Fragale, A., Bradley, T.E., Anselmi, M., Ciolfi, A., Cecchetti, S., Muto, V., *et al.* (2014). Mutations in ZBTB20 cause Primrose syndrome. Nat Genet *46*, 815-817.

Cossart, P., Boquet, P., Normark, S., and Rappuoli, R. (1996). Cellular microbiology emerging. Science *271*, 315-316.

Crosslin, D.R., Tromp, G., Burt, A., Kim, D.S., Verma, S.S., Lucas, A.M., Bradford, Y., Crawford, D.C., Armasu, S.M., Heit, J.A., *et al.* (2014). Controlling for population structure and genotyping platform bias in the eMERGE multi-institutional biobank linked to electronic health records. Frontiers in genetics *5*, 352.

Das, S., Forer, L., Schonherr, S., Sidore, C., Locke, A.E., Kwong, A., Vrieze, S.I., Chew, E.Y., Levy, S., McGue, M., *et al.* (2016). Next-generation genotype imputation service and methods. Nat Genet *48*, 1284-1287.

Datsenko, K.A., and Wanner, B.L. (2000). One-step inactivation of chromosomal genes in Escherichia coli K-12 using PCR products. Proc Natl Acad Sci U S A *97*, 6640-6645.

Dean, M., Carrington, M., Winkler, C., Huttley, G.A., Smith, M.W., Allikmets, R., Goedert, J.J., Buchbinder, S.P., Vittinghoff, E., Gomperts, E., *et al.* (1996). Genetic restriction of HIV-1 infection and progression to AIDS by a deletion allele of the CKR5 structural gene. Hemophilia Growth and Development Study, Multicenter AIDS Cohort Study, Multicenter Hemophilia Cohort Study, San Francisco City Cohort, ALIVE Study. Science *273*, 1856-1862.

Delaneau, O., Zagury, J.F., and Marchini, J. (2013). Improved whole-chromosome phasing for disease and population genetic studies. Nature methods *10*, 5-6.

Denny, J.C., Bastarache, L., Ritchie, M.D., Carroll, R.J., Zink, R., Mosley, J.D., Field, J.R., Pulley, J.M., Ramirez, A.H., Bowton, E., *et al.* (2013). Systematic comparison of phenome-wide association study of electronic medical record data and genome-wide association study data. Nature biotechnology *31*, 1102-1110.

Denny, J.C., Ritchie, M.D., Basford, M.A., Pulley, J.M., Bastarache, L., Brown-Gentry, K., Wang, D., Masys, D.R., Roden, D.M., and Crawford, D.C. (2010). PheWAS: demonstrating the feasibility of a phenome-wide scan to discover gene-disease associations. Bioinformatics *26*, 1205-1210.

Dougan, G., and Baker, S. (2014). Salmonella enterica serovar Typhi and the pathogenesis of typhoid fever. Annual review of microbiology *68*, 317-336.

Falconer, D.S., and Mackay, T.F.C. (1996). Introduction to Quantitative Genetics, 4 edn (Harlow, Essex, U.K.: Longmans Green).

Fisher, C.E., Hohl, T.M., Fan, W., Storer, B.E., Levine, D.M., Zhao, L.P., Martin, P.J., Warren, E.H., Boeckh, M., and Hansen, J.A. (2017). Validation of single nucleotide polymorphisms in invasive aspergillosis following hematopoietic cell transplantation. Blood *129*, 2693-2701.

Fletcher, N.F., Clark, A.R., Balfe, P., and McKeating, J.A. (2017). TNF superfamily members promote hepatitis C virus entry via an NF-kappaB and myosin light chain kinase dependent pathway. J Gen Virol *98*, 405-412.

Flutre, T., Wen, X., Pritchard, J., and Stephens, M. (2013). A statistical framework for joint eQTL analysis in multiple tissues. PLoS Genet *9*, e1003486.

Friedman, M.J. (1978). Erythrocytic mechanism of sickle cell resistance to malaria. Proc Natl Acad Sci U S A *75*, 1994-1997.

Fumagalli, M., Sironi, M., Pozzoli, U., Ferrer-Admetlla, A., Pattini, L., and Nielsen, R. (2011). Signatures of environmental genetic adaptation pinpoint pathogens as the main selective pressure through human evolution. PLoS Genet *7*, e1002355.

Furtado, J.M., Smith, J.R., Belfort, R., Jr., Gattey, D., and Winthrop, K.L. (2011). Toxoplasmosis: a global threat. J Glob Infect Dis *3*, 281-284.

Gottesman, O., Kuivaniemi, H., Tromp, G., Faucett, W.A., Li, R., Manolio, T.A., Sanderson, S.C., Kannry, J., Zinberg, R., Basford, M.A., *et al.* (2013). The Electronic Medical Records and Genomics (eMERGE) Network: past, present, and future. Genet Med *15*, 761-771.

Groom, J.R., and Luster, A.D. (2011). CXCR3 ligands: redundant, collaborative and antagonistic functions. Immunol Cell Biol *89*, 207-215.

Han, F., Yu, H., Li, P., Zhang, J., Tian, C., Li, H., and Zheng, Q.Y. (2012). Mutation in Phex gene predisposes BALB/c-Phex(Hyp-Duk)/Y mice to otitis media. PLoS One *7*, e43010.

Hennig, C., Ilginus, C., Boztug, K., Skokowa, J., Marodi, L., Szaflarska, A., Sass, M., Pignata, C., Kilic, S.S., Caragol, I., *et al.* (2014). High-content cytometry and transcriptomic biomarker profiling of human B-cell activation. J Allergy Clin Immunol *133*, 172-180 e171-110.

Hoff, S.T., Salman, A.M., Ruhwald, M., Ravn, P., Brock, I., Elsheikh, N., Andersen, P., and Agger, E.M. (2015). Human B cells produce chemokine CXCL10 in the presence of Mycobacterium tuberculosis specific T cells. Tuberculosis (Edinb) *95*, 40-47.

Howie, B., Fuchsberger, C., Stephens, M., Marchini, J., and Abecasis, G.R. (2012). Fast and accurate genotype imputation in genome-wide association studies through pre-phasing. Nat Genet *44*, 955-959.

Howie, B.N., Donnelly, P., and Marchini, J. (2009). A flexible and accurate genotype imputation method for the next generation of genome-wide association studies. PLoS Genet *5*, e1000529.

Hyun, J.G., Lee, G., Brown, J.B., Grimm, G.R., Tang, Y., Mittal, N., Dirisina, R., Zhang, Z., Fryer, J.P., Weinstock, J.V., *et al.* (2005). Anti-interferon-inducible chemokine, CXCL10, reduces colitis by impairing T helper-1 induction and recruitment in mice. Inflammatory bowel diseases *11*, 799-805.

International HapMap, C., Altshuler, D.M., Gibbs, R.A., Peltonen, L., Altshuler, D.M., Gibbs, R.A., Peltonen, L., Dermitzakis, E., Schaffner, S.F., Yu, F., *et al.* (2010). Integrating common and rare genetic variation in diverse human populations. Nature *467*, 52-58.

Iotchkova, V., Ritchie, G.R.S., Geihs, M., Morganella, S., Min, J.L., Walter, K., Timpson, N.J., Consortium, U.K., Dunham, I., Birney, E., *et al.* (2016). GARFIELD--GWAS Analysis of Regulatory or Functional Information Enrichment with LD correction. bioRxiv *doi: 10.1101/085738*

Kato, A., Ogasawara, T., Homma, T., Batchelor, J., Imai, S., Wakiguchi, H., Saito, H., and Matsumoto, K. (2004). CpG oligodeoxynucleotides directly induce CXCR3 chemokines in human B cells. Biochemical and biophysical research communications *320*, 1139-1147.

Kaur, R., Casey, J., and Pichichero, M. (2015). Cytokine, chemokine, and Toll-like receptor expression in middle ear fluids of children with acute otitis media. Laryngoscope *125*, E39-44.

Kirk, M.D., Pires, S.M., Black, R.E., Caipo, M., Crump, J.A., Devleesschauwer, B., Dopfer, D., Fazil, A., Fischer-Walker, C.L., Hald, T., *et al.* (2015). World Health Organization Estimates of the Global and Regional Disease Burden of 22 Foodborne Bacterial, Protozoal, and Viral Diseases, 2010: A Data Synthesis. PLoS Med *12*, e1001921.

Ko, D.C., Gamazon, E.R., Shukla, K.P., Pfuetzner, R.A., Whittington, D., Holden, T.D., Brittnacher, M.J., Fong, C., Radey, M., Ogohara, C., *et al.* (2012). Functional genetic screen of human diversity reveals that a methionine salvage enzyme regulates inflammatory cell death. Proc Natl Acad Sci U S A *109*, E2343-2352.

Ko, D.C., Shukla, K.P., Fong, C., Wasnick, M., Brittnacher, M.J., Wurfel, M.M., Holden, T.D., O'Keefe, G.E., Van Yserloo, B., Akey, J.M., *et al.* (2009). A genome-wide in vitro bacterial-infection screen reveals human variation in the host response associated with inflammatory disease. Am J Hum Genet *85*, 214-227.

Ko, D.C., and Urban, T.J. (2013). Understanding Human Variation in Infectious Disease Susceptibility through Clinical and Cellular GWAS. PLoS Pathog *9*, e1003424.

Lee, S.C., Billmyre, R.B., Li, A., Carson, S., Sykes, S.M., Huh, E.Y., Mieczkowski, P., Ko, D.C., Cuomo, C.A., and Heitman, J. (2014). Analysis of a food-borne fungal pathogen outbreak: virulence and genome of a Mucor circinelloides isolate from yogurt. MBio *5*, e01390-01314.

Lee, S.C., Li, A., Calo, S., Inoue, M., Tonthat, N.K., Bain, J.M., Louw, J., Shinohara, M.L., Erwig, L.P., Schumacher, M.A., *et al.* (2015). Calcineurin orchestrates dimorphic transitions,

antifungal drug responses and host-pathogen interactions of the pathogenic mucoralean fungus Mucor circinelloides. Molecular microbiology *97*, 844-865.

Li, C.H., Cervantes, M., Springer, D.J., Boekhout, T., Ruiz-Vazquez, R.M., Torres-Martinez, S.R., Heitman, J., and Lee, S.C. (2011). Sporangiospore Size Dimorphism Is Linked to Virulence of Mucor circinelloides. Plos Pathogens *7*.

Li, H., Handsaker, B., Wysoker, A., Fennell, T., Ruan, J., Homer, N., Marth, G., Abecasis, G., Durbin, R., and Genome Project Data Processing, S. (2009). The Sequence Alignment/Map format and SAMtools. Bioinformatics *25*, 2078-2079.

Li, J.Z., Absher, D.M., Tang, H., Southwick, A.M., Casto, A.M., Ramachandran, S., Cann, H.M., Barsh, G.S., Feldman, M., Cavalli-Sforza, L.L., *et al.* (2008). Worldwide human relationships inferred from genome-wide patterns of variation. Science *319*, 1100-1104.

Li, Y., Oosting, M., Smeekens, S.P., Jaeger, M., Aguirre-Gamboa, R., Le, K.T., Deelen, P., Ricano-Ponce, I., Schoffelen, T., Jansen, A.F., *et al.* (2016). A Functional Genomics Approach to Understand Variation in Cytokine Production in Humans. Cell *167*, 1099-1110 e1014.

Liu, J.Z., van Sommeren, S., Huang, H., Ng, S.C., Alberts, R., Takahashi, A., Ripke, S., Lee, J.C., Jostins, L., Shah, T., *et al.* (2015). Association analyses identify 38 susceptibility loci for inflammatory bowel disease and highlight shared genetic risk across populations. Nat Genet *47*, 979-986.

Liu, R., Paxton, W.A., Choe, S., Ceradini, D., Martin, S.R., Horuk, R., MacDonald, M.E., Stuhlmann, H., Koup, R.A., and Landau, N.R. (1996). Homozygous defect in HIV-1 coreceptor accounts for resistance of some multiply-exposed individuals to HIV-1 infection. Cell *86*, 367-377.

Liu, X., Zhang, P., Bao, Y., Han, Y., Wang, Y., Zhang, Q., Zhan, Z., Meng, J., Li, Y., Li, N., *et al.* (2013). Zinc finger protein ZBTB20 promotes Toll-like receptor-triggered innate immune responses by repressing IkappaBalpha gene transcription. Proc Natl Acad Sci U S A *110*, 11097-11102.

Loh, P.R., Danecek, P., Palamara, P.F., Fuchsberger, C., Y, A.R., H, K.F., Schoenherr, S., Forer, L., McCarthy, S., Abecasis, G.R., *et al.* (2016). Reference-based phasing using the Haplotype Reference Consortium panel. Nat Genet *48*, 1443-1448.

Majowicz, S.E., Musto, J., Scallan, E., Angulo, F.J., Kirk, M., O'Brien, S.J., Jones, T.F., Fazil, A., Hoekstra, R.M., and International Collaboration on Enteric Disease 'Burden of Illness, S. (2010). The global burden of nontyphoidal Salmonella gastroenteritis. Clinical infectious diseases : an official publication of the Infectious Diseases Society of America *50*, 882-889.

Marcus, J.H., and Novembre, J. (2017). Visualizing the geography of genetic variants. Bioinformatics *33*, 594-595.

McCarthy, S., Das, S., Kretzschmar, W., Delaneau, O., Wood, A.R., Teumer, A., Kang, H.M., Fuchsberger, C., Danecek, P., Sharp, K., *et al.* (2016). A reference panel of 64,976 haplotypes for genotype imputation. Nat Genet *48*, 1279-1283.

McCarty, C.A., Chisholm, R.L., Chute, C.G., Kullo, I.J., Jarvik, G.P., Larson, E.B., Li, R., Masys, D.R., Ritchie, M.D., Roden, D.M., *et al.* (2011). The eMERGE Network: a consortium of biorepositories linked to electronic medical records data for conducting genomic studies. BMC Med Genomics *4*, 13.

McDavid, A., Crane, P.K., Newton, K.M., Crosslin, D.R., McCormick, W., Weston, N., Ehrlich, K., Hart, E., Harrison, R., Kukull, W.A., *et al.* (2013). Enhancing the power of genetic association studies through the use of silver standard cases derived from electronic medical records. PLoS One *8*, e63481.

Mendoza, L., Vilela, R., Voelz, K., Ibrahim, A.S., Voigt, K., and Lee, S.C. (2014). Human Fungal Pathogens of Mucorales and Entomophthorales. Cold Spring Harb Perspect Med *5*.

Mezger, M., Steffens, M., Beyer, M., Manger, C., Eberle, J., Toliat, M.R., Wienker, T.F., Ljungman, P., Hebart, H., Dornbusch, H.J., *et al.* (2008). Polymorphisms in the chemokine (C-X-C motif) ligand 10 are associated with invasive aspergillosis after allogeneic stem-cell transplantation and influence CXCL10 expression in monocyte-derived dendritic cells. Blood *111*, 534-536.

Mitchelmore, C., Kjaerulff, K.M., Pedersen, H.C., Nielsen, J.V., Rasmussen, T.E., Fisker, M.F., Finsen, B., Pedersen, K.M., and Jensen, N.A. (2002). Characterization of two novel nuclear BTB/POZ domain zinc finger isoforms. Association with differentiation of hippocampal neurons, cerebellar granule cells, and macroglia. J Biol Chem *277*, 7598-7609.

Newman, L., Rowley, J., Vander Hoorn, S., Wijesooriya, N.S., Unemo, M., Low, N., Stevens, G., Gottlieb, S., Kiarie, J., and Temmerman, M. (2015). Global Estimates of the Prevalence and Incidence of Four Curable Sexually Transmitted Infections in 2012 Based on Systematic Review and Global Reporting. PLoS One *10*, e0143304.

Nica, A.C., and Dermitzakis, E.T. (2013). Expression quantitative trait loci: present and future. Philosophical transactions of the Royal Society of London Series B, Biological sciences *368*, 20120362.

Nielsen, J.V., Nielsen, F.H., Ismail, R., Noraberg, J., and Jensen, N.A. (2007). Hippocampus-like corticoneurogenesis induced by two isoforms of the BTB-zinc finger gene Zbtb20 in mice. Development *134*, 1133-1140.

Nogueira, L.G., Santos, R.H., Ianni, B.M., Fiorelli, A.I., Mairena, E.C., Benvenuti, L.A., Frade, A., Donadi, E., Dias, F., Saba, B., *et al.* (2012). Myocardial chemokine expression and intensity of myocarditis in Chagas cardiomyopathy are controlled by polymorphisms in CXCL9 and CXCL10. PLoS Negl Trop Dis *6*, e1867.

Odds, F.C., Brown, A.J., and Gow, N.A. (2004). Candida albicans genome sequence: a platform for genomics in the absence of genetics. Genome biology *5*, 230.

Orru, V., Steri, M., Sole, G., Sidore, C., Virdis, F., Dei, M., Lai, S., Zoledziewska, M., Busonero, F., Mulas, A., *et al.* (2013). Genetic Variants Regulating Immune Cell Levels in Health and Disease. Cell *155*, 242-256.

Ostvik, A.E., Granlund, A.V., Bugge, M., Nilsen, N.J., Torp, S.H., Waldum, H.L., Damas, J.K., Espevik, T., and Sandvik, A.K. (2013). Enhanced expression of CXCL10 in inflammatory bowel disease: potential role of mucosal Toll-like receptor 3 stimulation. Inflammatory bowel diseases *19*, 265-274.

Parkhill, J., Dougan, G., James, K.D., Thomson, N.R., Pickard, D., Wain, J., Churcher, C., Mungall, K.L., Bentley, S.D., Holden, M.T., *et al.* (2001). Complete genome sequence of a multiple drug resistant Salmonella enterica serovar Typhi CT18. Nature *413*, 848-852.

Pickrell, J.K., and Reich, D. (2014). Toward a new history and geography of human genes informed by ancient DNA. Trends Genet *30*, 377-389.

Pineda-Tenor, D., Berenguer, J., Garcia-Alvarez, M., Guzman-Fulgencio, M., Carrero, A., Aldamiz-Echevarria, T., Tejerina, F., Diez, C., Jimenez-Sousa, M.A., Fernandez-Rodriguez, A., *et al.* (2015). Single nucleotide polymorphisms of CXCL9-11 chemokines are associated with liver fibrosis in HIV/HCV-coinfected patients. J Acquir Immune Defic Syndr *68*, 386-395.

Pineda-Tenor, D., Berenguer, J., Jimenez-Sousa, M.A., Guzman-Fulgencio, M., Aldamiz-Echevarria, T., Carrero, A., Garcia-Alvarez, M., Diez, C., Tejerina, F., Briz, V., *et al.* (2014).

CXCL9, CXCL10 and CXCL11 polymorphisms are associated with sustained virologic response in HIV/HCV-coinfected patients. J Clin Virol *61*, 423-429.

Pittman, K.J., Glover, L.C., Wang, L., and Ko, D.C. (2016). The Legacy of Past Pandemics: Common Human Mutations That Protect against Infectious Disease. PLoS Pathog *12*, e1005680.

Pruim, R.J., Welch, R.P., Sanna, S., Teslovich, T.M., Chines, P.S., Gliedt, T.P., Boehnke, M., Abecasis, G.R., and Willer, C.J. (2010). LocusZoom: regional visualization of genome-wide association scan results. Bioinformatics *26*, 2336-2337.

Pujol, C., and Bliska, J.B. (2003). The ability to replicate in macrophages is conserved between Yersinia pestis and Yersinia pseudotuberculosis. Infect Immun *71*, 5892-5899.

Purcell, S., Neale, B., Todd-Brown, K., Thomas, L., Ferreira, M.A., Bender, D., Maller, J., Sklar, P., de Bakker, P.I., Daly, M.J., *et al.* (2007). PLINK: a tool set for whole-genome association and population-based linkage analyses. Am J Hum Genet *81*, 559-575.

Purcell, S., Sham, P., and Daly, M.J. (2005). Parental phenotypes in family-based association analysis. Am J Hum Genet *76*, 249-259.

Roederer, M., Quaye, L., Mangino, M., Beddall, M.H., Mahnke, Y., Chattopadhyay, P., Tosi, I., Napolitano, L., Terranova Barberio, M., Menni, C., *et al.* (2015). The genetic architecture of the human immune system: a bioresource for autoimmunity and disease pathogenesis. Cell *161*, 387-403.

Roncero, M.I.G. (1984). Enrichment method for the isolation of auxotrophic mutants of Mucor using the polyene antibiotic N-glycosyl-polifungin. Carlsberg Research Communications *49*, 685.

Saeij, J.P., Boyle, J.P., Grigg, M.E., Arrizabalaga, G., and Boothroyd, J.C. (2005). Bioluminescence imaging of Toxoplasma gondii infection in living mice reveals dramatic differences between strains. Infect Immun *73*, 695-702.

Saka, H.A., Thompson, J.W., Chen, Y.S., Kumar, Y., Dubois, L.G., Moseley, M.A., and Valdivia, R.H. (2011). Quantitative proteomics reveals metabolic and pathogenic properties of Chlamydia trachomatis developmental forms. Molecular microbiology *82*, 1185-1203.

Samson, M., Libert, F., Doranz, B.J., Rucker, J., Liesnard, C., Farber, C.M., Saragosti, S., Lapoumeroulie, C., Cognaux, J., Forceille, C., *et al.* (1996). Resistance to HIV-1 infection in caucasian individuals bearing mutant alleles of the CCR-5 chemokine receptor gene. Nature *382*, 722-725.

Sandborn, W.J., Colombel, J.F., Ghosh, S., Sands, B.E., Dryden, G., Hebuterne, X., Leong, R.W., Bressler, B., Ullman, T., Lakatos, P.L., *et al.* (2016). Eldelumab [Anti-IP-10] Induction Therapy for Ulcerative Colitis: A Randomised, Placebo-Controlled, Phase 2b Study. J Crohns Colitis *10*, 418-428.

Sandborn, W.J., Rutgeerts, P., Colombel, J.F., Ghosh, S., Petryka, R., Sands, B.E., Mitra, P., and Luo, A. (2017). Eldelumab [anti-interferon-gamma-inducible protein-10 antibody] Induction Therapy for Active Crohn's Disease: a Randomised, Double-blind, Placebo-controlled Phase IIa Study. J Crohns Colitis.

Sasaki, S., Yoneyama, H., Suzuki, K., Suriki, H., Aiba, T., Watanabe, S., Kawauchi, Y., Kawachi, H., Shimizu, F., Matsushima, K., *et al.* (2002). Blockade of CXCL10 protects mice from acute colitis and enhances crypt cell survival. Eur J Immunol *32*, 3197-3205.

Shih, B., and Bayat, A. (2010). Genetics of keloid scarring. Arch Dermatol Res *302*, 319-339.

Singh, U.P., Singh, S., Taub, D.D., and Lillard, J.W., Jr. (2003). Inhibition of IFN-gamma-inducible protein-10 abrogates colitis in IL-10-/- mice. J Immunol *171*, 1401-1406.

Solovieff, N., Cotsapas, C., Lee, P.H., Purcell, S.M., and Smoller, J.W. (2013). Pleiotropy in complex traits: challenges and strategies. Nature reviews Genetics *14*, 483-495.

Staples, J., Nickerson, D.A., and Below, J.E. (2013). Utilizing graph theory to select the largest set of unrelated individuals for genetic analysis. Genet Epidemiol *37*, 136-141.

Staples, J., Qiao, D., Cho, M.H., Silverman, E.K., University of Washington Center for Mendelian, G., Nickerson, D.A., and Below, J.E. (2014). PRIMUS: rapid reconstruction of pedigrees from genome-wide estimates of identity by descent. Am J Hum Genet *95*, 553-564.

Stranger, B.E., Montgomery, S.B., Dimas, A.S., Parts, L., Stegle, O., Ingle, C.E., Sekowska, M., Smith, G.D., Evans, D., Gutierrez-Arcelus, M., *et al.* (2012). Patterns of cis regulatory variation in diverse human populations. PLoS Genet *8*, e1002639.

Stranger, B.E., Nica, A.C., Forrest, M.S., Dimas, A., Bird, C.P., Beazley, C., Ingle, C.E., Dunning, M., Flicek, P., Koller, D., *et al.* (2007). Population genomics of human gene expression. Nat Genet *39*, 1217-1224.

Team, R.C. (2016). R: A language and environment for statistical computing. R Foundation for Statistical Computing, Vienna, Austria. URL: http://www.R-project.org/.

Tong, H.H., Long, J.P., Shannon, P.A., and DeMaria, T.F. (2003). Expression of cytokine and chemokine genes by human middle ear epithelial cells induced by influenza A virus and Streptococcus pneumoniae opacity variants. Infect Immun *71*, 4289-4296.

Tong, S.Y., Davis, J.S., Eichenberger, E., Holland, T.L., and Fowler, V.G., Jr. (2015). Staphylococcus aureus infections: epidemiology, pathophysiology, clinical manifestations, and management. Clin Microbiol Rev *28*, 603-661.

Uguccioni, M., Gionchetti, P., Robbiani, D.F., Rizzello, F., Peruzzo, S., Campieri, M., and Baggiolini, M. (1999). Increased expression of IP-10, IL-8, MCP-1, and MCP-3 in ulcerative colitis. Am J Pathol *155*, 331-336.

Visscher, P.M., Hill, W.G., and Wray, N.R. (2008). Heritability in the genomics era--concepts and misconceptions. Nature reviews Genetics *9*, 255-266.

Vollmer, J., Jurk, M., Samulowitz, U., Lipford, G., Forsbach, A., Wullner, M., Tluk, S., Hartmann, H., Kritzler, A., Muller, C., *et al.* (2004). CpG oligodeoxynucleotides stimulate IFN-gamma-inducible protein-10 production in human B cells. J Endotoxin Res *10*, 431-438.

Wang, K., Li, M., and Hakonarson, H. (2010). ANNOVAR: functional annotation of genetic variants from high-throughput sequencing data. Nucleic acids research *38*, e164.

Wang, L., Ko, E.R., Gilchrist, J.J., Pittman, K.J., Rautanen, A., Pirinen, M., Thompson, J.W., Dubois, L.G., Langley, R.G., Jaslow, S.L., *et al.* (2017). Human genetic and metabolite variation reveal methylthioadenosine is a prognostic biomarker and inflammatory regulator in sepsis. Science Advances *3*, e1602096.

Welter, D., MacArthur, J., Morales, J., Burdett, T., Hall, P., Junkins, H., Klemm, A., Flicek, P., Manolio, T., Hindorff, L., *et al.* (2014). The NHGRI GWAS Catalog, a curated resource of SNP-trait associations. Nucleic acids research *42*, D1001-1006.

Wolfe, D., Dudek, S., Ritchie, M.D., and Pendergrass, S.A. (2013). Visualizing genomic information across chromosomes with PhenoGram. BioData Min *6*, 18.

Wynn, T.A., and Ramalingam, T.R. (2012). Mechanisms of fibrosis: therapeutic translation for fibrotic disease. Nature medicine *18*, 1028-1040.

Xie, Z., Zhang, H., Tsai, W., Zhang, Y., Du, Y., Zhong, J., Szpirer, C., Zhu, M., Cao, X., Barton, M.C., *et al.* (2008). Zinc finger protein ZBTB20 is a key repressor of alpha-fetoprotein gene transcription in liver. Proc Natl Acad Sci U S A *105*, 10859-10864.

Xu, W., Joo, H., Clayton, S., Dullaers, M., Herve, M.C., Blankenship, D., De La Morena, M.T., Balderas, R., Picard, C., Casanova, J.L., *et al.* (2012). Macrophages induce differentiation of plasma cells through CXCL10/IP-10. J Exp Med *209*, 1813-1823, S1811-1812.

Yang, J., Lee, S.H., Goddard, M.E., and Visscher, P.M. (2011). GCTA: a tool for genome-wide complex trait analysis. Am J Hum Genet *88*, 76-82.

Yapar, N. (2014). Epidemiology and risk factors for invasive candidiasis. Ther Clin Risk Manag *10*, 95-105.

Zaitlen, N., Kraft, P., Patterson, N., Pasaniuc, B., Bhatia, G., Pollack, S., and Price, A.L. (2013). Using extended genealogy to estimate components of heritability for 23 quantitative and dichotomous traits. PLoS Genet *9*, e1003520.

Figures

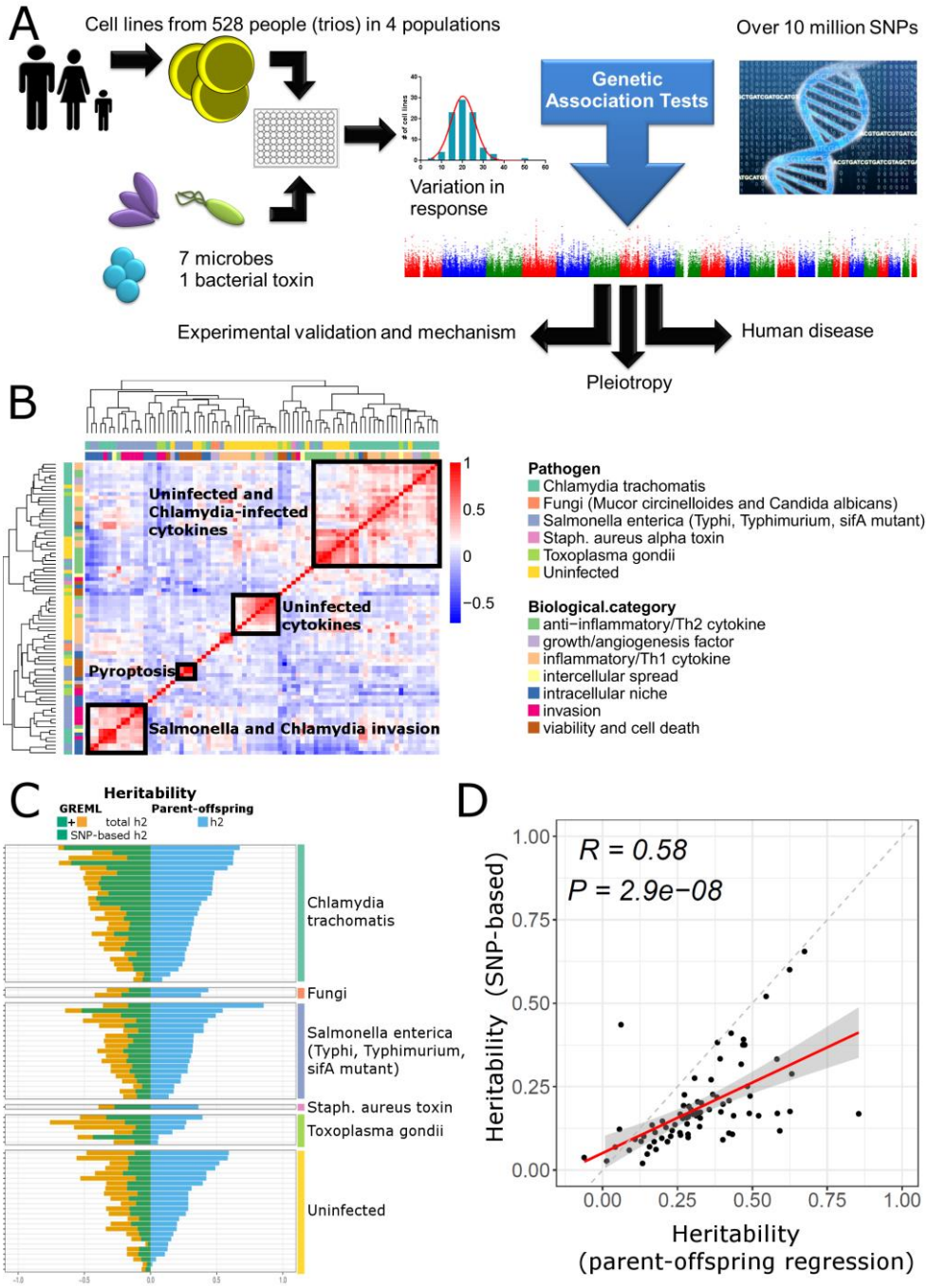

Figure 1. Inter-individual variation in H2P2 traits reveals clustering of phenotypes and heritable variation in cellular responses to infection. (A) Diagram of the H2P2 workflow for connecting genetic variation to cell biology. Lymphoblastoid cell lines (LCLs) from 528 people

(parent-offspring trios) from 4 populations were exposed to 8 different stimuli for 79 phenotypes. Over 10 million SNPs were tested for association with each phenotype using family-based association implemented in PLINK (Purcell et al., 2007; Purcell et al., 2005). (B) Clustering of H2P2 phenotypes reveals a map of trait similarity. Heatmap and dendograms of hierarchical clustering based on inter-individual phenotypic variation. Spearman correlation is color-coded in the heatmap from blue (negative correlation) to red (positive correlation). Phenotypes are color-coded by stimuli (outer band) and biological category of phenotype (inner band). Several clusters of related traits are highlighted. (C) Narrow-sense heritability (h^2) estimates for H2P2 phenotypes based on GREML vs. parent-offspring regression. h^2 was estimated using genome-wide SNP data using the Zaitlen method of GREML for family data in GCTA or by parent-offspring regression. Both methods utilized a covariate for batch effects. The GREML method gives a SNP-based h^2 (green) as well as a total h^2 (yellow; the sum of SNP-based h^2 (green) plus the non-SNP-based h^2). Both methods indicate a large range of h^2 estimates for different H2P2 traits and are consistent with many traits having a significant genetic component. (D) h^2 estimates from parent-offspring regression vs. GREML SNP-based h^2 are well correlated. Linear regression for all 79 H2P2 traits demonstrate the two methods give similar h^2 estimates ($r=0.58$, $p=2.9\times10^{-8}$).

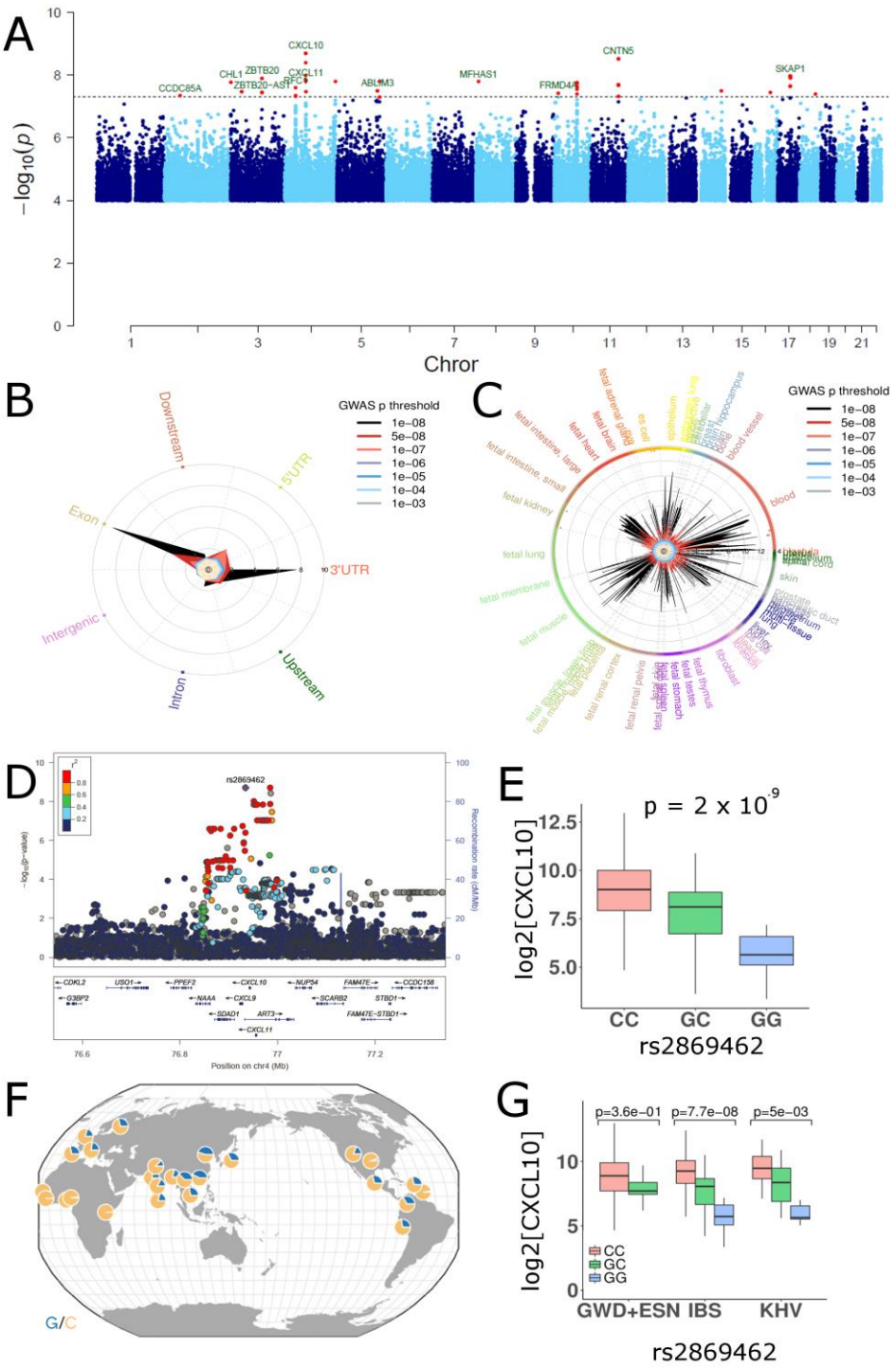

795

Figure 2. GWA of H2P2 reveals 17 genome-wide significant loci including a cis-cytokine-QTL near *CXCL10*. (A) A meta-Manhattan plot for 79 traits shows 17 peaks (red) with $p<5x10^{-8}$ (dotted line). –log(p-values) were calculated using QFAM-parents in PLINK. (B) GARFIELD

enrichment plot of SNP location demonstrates enrichment of SNPs associated with H2P2 phenotypes in exons, and 5' and 3' UTRs. SNPs associated with H2P2 traits at various p-value thresholds were plotted in the indicated colors and the height of the peak within each category indicates fold enrichment from 0 to 10. (C) GARFIELD enrichment plot of DNase hypersensitivity peaks demonstrates enrichment of SNPs associated with H2P2 phenotypes in active chromatin regions in multiple cell/tissue types. SNPs associated with H2P2 traits at various p-value thresholds were plotted in the indicated colors and the height of the peak within each category indicates fold enrichment from 0 to 14. (D) Regional plot around the *CXCL10* gene demonstrates association of rs2869462 with CXCL10 levels from *C. trachomatis*-infected cells ($p=2x10^{-9}$). SNPs are plotted by position on chromosome 4 and –log(p-value) and color-coded by r^2 value to rs2869462 from 1000 Genomes European data. (E) Genotypic medians, first and third quartiles (box), and maximum and minimum values (whiskers) for rs2869462 for CXCL10 levels from *C. trachomatis*-infected LCLs from all LCLs. (F) Map of rs2869462 allele frequencies (C = orange; G = blue). (G) Individual population genotypic median plots for rs2869462 for CXCL10 levels demonstrate C > G in all populations. P-values are from QFAM-parents in PLINK.

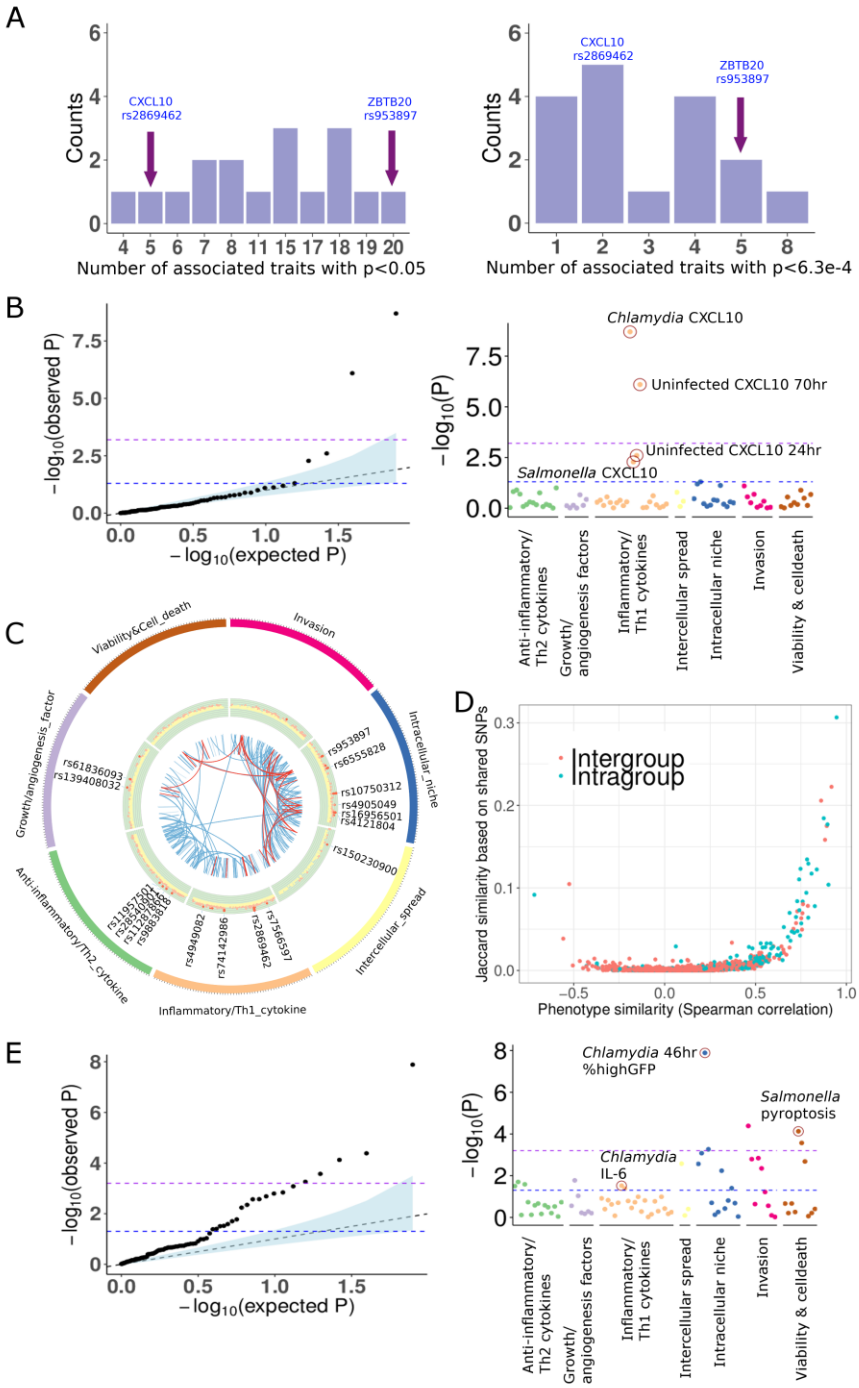

815

Figure 3. Cross-phenotype associations and pleiotropy are abundant among cellular host-pathogen traits. (A) Histograms of the number of cross-phenotype associations for the 17 H2P2 genome-wide significant hits. For the most strongly associated SNP in each GWAS peak, the

number of traits with associations at $p<0.05$ and $p<6.33x10^{-4}$ is shown. (B) QQ-plot and PheWAS plot for the association of rs2869462 with the 79 H2P2 phenotypes shows deviation from neutral expectation only for the 4 CXCL10 phenotypes. This is an example of cross-phenotype associations but not pleiotropy. (C) Circle plot of 79 phenotypes by category and lines connecting traits that share the same genome-wide significant hit at $p< 1x10^{-5}$. (D) Plot of pairwise trait phenotypic similarity (Spearman correlation) vs. similarity of shared SNPs (Jaccard index). Traits that are more phenotypically similar have more shared SNPs with $p< 1x10^{-3}$ for both traits. (E) QQ-plot and PheWAS plot for the association of rs953897 with the 79 H2P2 phenotypes shows deviation from neutral expectation for dozens of phenotypes, including traits in different biological categories in the PheWAS plot. This is an example of pleiotropy.

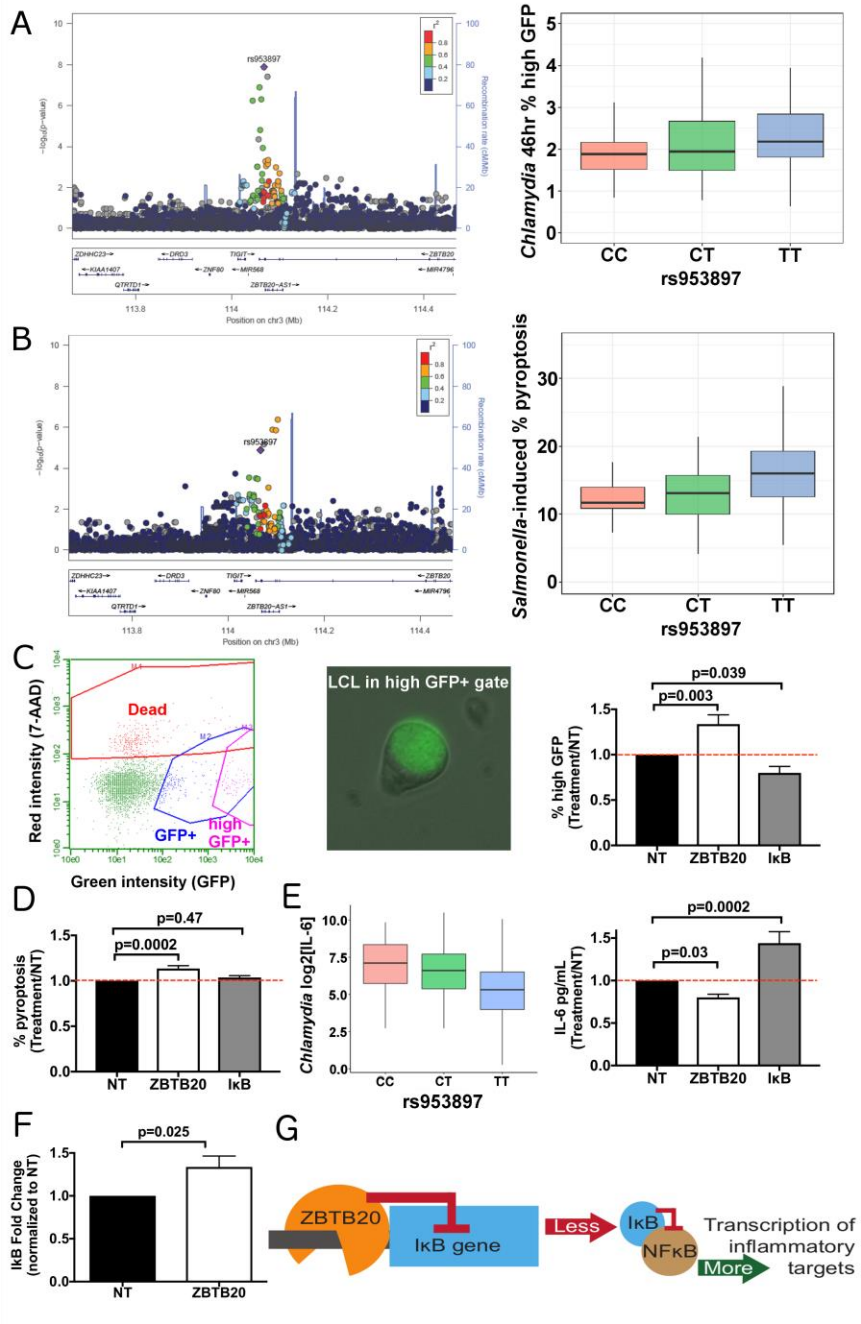

Figure 4. Genetic variation influencing *ZBTB20* regulates multiple host-pathogen traits. (A) Regional plot for *ZBTB20* demonstrates an association of rs953897 with *C. trachomatis* high GFP infected cells at 46 hrs ($p=1.3x10^{-8}$). Genotypic medians plot of rs953897 with high GFP infected cells at 46 hrs in IBS LCLs. (B) Regional plot for ZBTB20 demonstrates an association of rs953897 with *S.* Typhimurium-induced pyroptosis ($p=7.5x10^{-5}$). Genotypic medians plot of

rs953897 with *S.* Typhimurium-induced pyroptosis in all LCLs. (C-F) LCL GM1761 was treated with non-targeting, ZBTB20 (53±9% knockdown), or IκB (83±2% knockdown) Accell RNAi for three days prior to infection. All cellular phenotypes measured were normalized to non-targeting values (treatment/non-targeting) prior to statistical analysis. (C) ZBTB20 and IκB regulate *C. trachomatis* replication. By 46hrs, *C. trachomatis* replication has resulted in a high GFP+ population of cells with an enlarged GFP+ *Chlamydia*-containing vacuole. ZBTB20 knockdown resulted in a greater percentage of high GFP+ cells, similar to what is seen with the T allele, while IκB knockdown produces fewer GFP+ enlarged vacuoles. Mean (±SEM) percentage of high GFP+ cells in non-targeting samples is 1.63% (±0.07%). (D) ZBTB20 regulates *Salmonella*-induced pyroptosis independent of IκB. ZBTB20 knockdown results in a greater percentage of pyroptotic cells, similar to what is seen with the T allele, while IκB knockdown shows no significant change in pyroptosis. Percentage of pyroptotic cells in non-targeting samples is 35.1% (±1.41%). (E) Both the T allele and ZBTB20 knockdown result in reduced IL-6. Genotypic median plot of rs953897 with *C. trachomatis*-induced IL-6 in all LCLs. ZBTB20 knockdown reduces IL-6 levels, while knockdown of IκB leads to increased levels measured at 70 hours. IL-6 levels from non-targeting LCLs were 186 pg/mL (±31.55 pg/mL). (F) ZBTB20 knockdown results in increased IκB mRNA. RNA was collected from nontargeting and ZBTB20 RNAi treated LCLs, cDNA was synthesized, and qPCR was conducted using TaqMan probes for 18s (control) and IκB (target). The ΔΔCT method was used to determine fold change of IκB. (G) Proposed model for ZBTB20 effect on proinflammatory targets. C-F were from 8-12 biological replicates from 2-4 experiments. p-values for C and D were generated from one-way ANOVA analysis while F was calculated by an unpaired parametric t-test.

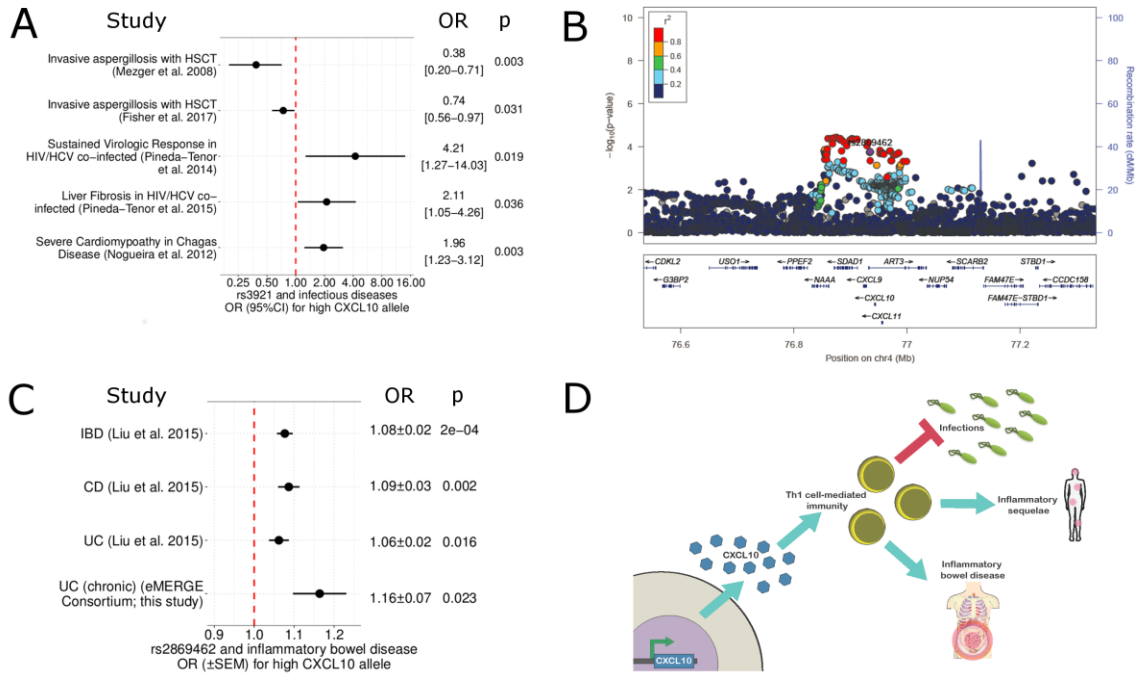

Figure 5. SNPs associated with high CXCL10 in H2P2 are also associated with decreased infectious disease risk, increased inflammatory sequelae, and increased risk of IBD. (A) Odds ratio (OR) plot for rs3921 and published infectious disease associations. rs3921 is in LD with rs2869462 (r^2=0.3 in Europeans) and is associated with *Chlamydia*-infected CXCL10 levels in H2P2 ($p=6.4x10^{-4}$). The high CXCL10 allele (C) is associated with reduced odds of infectious disease but greater odds of inflammatory sequelae. (B) Locuszoom plot for inflammatory bowel disease and *CXCL10* from GWAS of European ancestry conducting by the International Inflammatory Bowel Disease Genetics Consortium (Liu et al., 2015). rs2869462 is in a region demonstrating association not previously reported ($p=1.7x10^{-4}$; OR=1.08). (C) OR plot for rs2869462 and IBD, CD and UC based on data generated in (Liu et al., 2015) and replication of the association with UC from the eMERGE Network. The high CXCL10 allele (C) is associated with increased odds of IBD. (D) Model of levels of CXCL10 production promoting Th1 cell-

mediated immunity to inhibit certain infections but also resulting in increased inflammatory sequelae and risk of autoimmune conditions such as IBD.

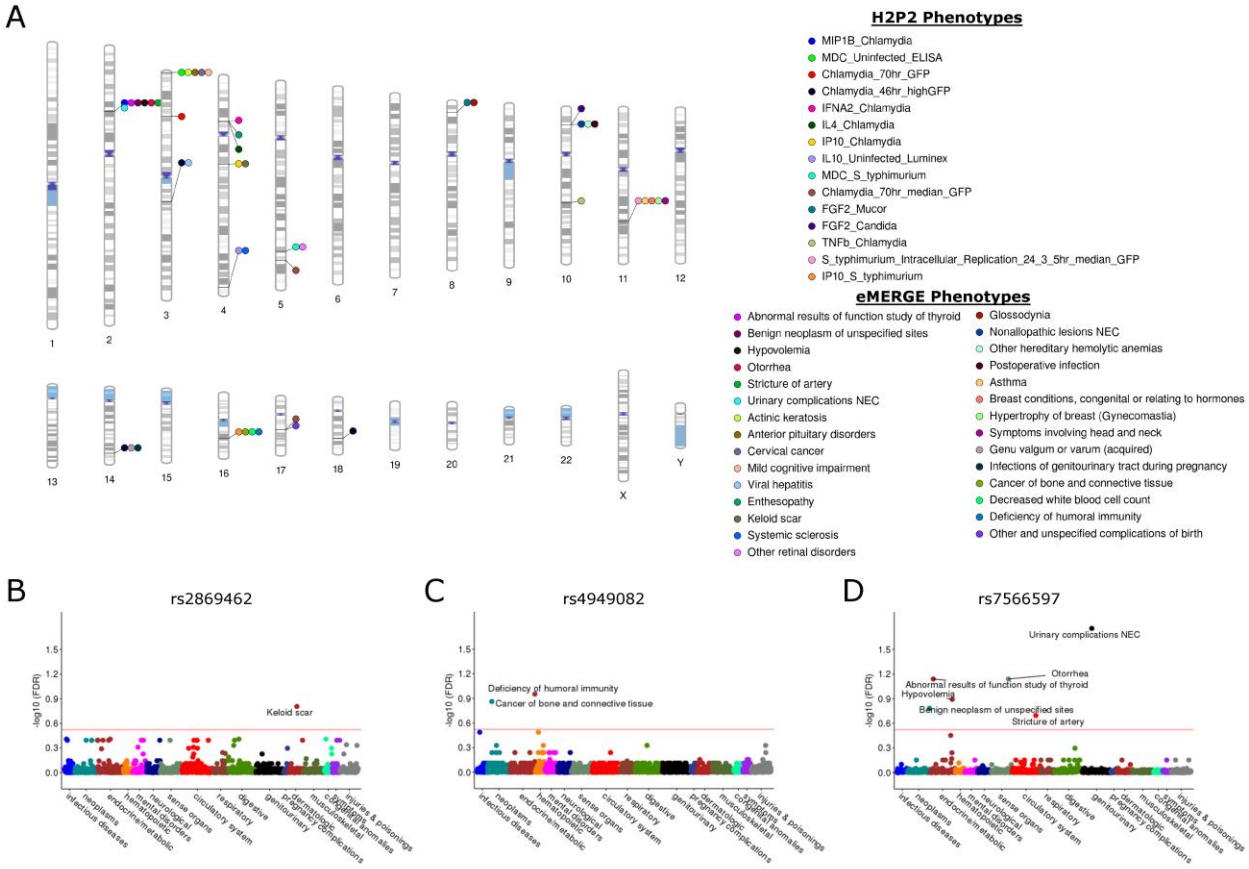

Figure 6. PheWAS of H2P2 hits reveals connections to human disease. (A) Phenogram plot of H2P2 genome-wide significant hits ($p<5x10^{-8}$) along with eMERGE phenotypes that demonstrate an association (FDR < 0.3) with these same SNPs. The color of the first circle at each locus is coded for the H2P2 showing an association. Additional circles at each locus are colored according to the eMERGE phenotype(s) that shows an association. Image created and modified from (Wolfe et al., 2013). (B) (C) (D) eMERGE PheWAS plots of 3 SNPs identified by H2P2. eMERGE phenotypes are grouped into functional categories. Y-axis is –log(FDR), with the red line indicating FDR < 0.3.

Table 1. Genome-wide-significant H2P2 SNPs. A single SNP with the lowest p-value is listed for each peak. SNPs described in detail in the text are in bold.

SNP ID	Chr	Position	Cellular trait	p-value	risk allele	gene*	Parent-offspring h^2 for trait	SNP-based h^2 for trait	variance explained by SNP (parental LCLs only)
rs7566597	**2**	**56289463**	**MIP1B_Chlamydia**	**4.67E-08**	**G**	**CCDC85A**	**58.2%**	**33.3%**	**4.4%**
rs9883818	3	337848	MDC_Uninfected_ELISA	1.70E-08	A	CHL1	28.6%	9.8%	1.2%
rs150230900	3	38822664	Chlamydia_70hr_GFP	3.50E-08	-	near RP11-134J21.1	21.1%	12.9%	1.0%
rs953897	**3**	**114349113**	**Chlamydia_46hr_highGFP**	**1.30E-08**	**T**	**ZBTB20**	**33.0%**	**20.1%**	**2.4%**
rs11287866	4	39317796	IL4_Chlamydia	2.60E-08	TA	RFC1	36.8%	22.7%	1.6%
rs2869462	**4**	**76013566**	**IP10_Chlamydia**	**2.00E-09**	**C**	**ART3; near CXCL10**	**48.3%**	**25.2%**	**13.7%**
rs28540901	4	184492384	IL10_Uninfected_Luminex	1.60E-08	T	near IRF2	10.8%	9.2%	2.9%
rs11957501	5	149250737	MDC_S_typhimurium	3.25E-08	C	ABLIM3	43.3%	10.7%	4.9%
rs6555828	5	157066729	Chlamydia_70hr_median_GFP	1.60E-08	G	near HAVCR1	27.3%	22.6%	2.8%
rs139408032	8	8882324	FGF2_Mucor	1.65E-08	A	MFHAS1	38.2%	21.9%	2.7%
rs61836093	10	14235152	FGF2_Candida	3.80E-08	G	FRMD4A	43.7%	16.3%	2.0%
rs74142986	10	81018235	TNFb_Chlamydia	1.85E-08	T	-	35.6%	18.2%	2.5%
rs10750312	11	99526242	S_typhimurium_Intracellular_Replication_24_3_5hr_median_GFP	3.00E-09	G	CNTN5	22.7%	10.2%	3.2%
rs4905049	14	93121941	Chlamydia_46hr_highGFP	3.30E-08	G	near ITPK1	33.0%	20.1%	0.3%
rs4949082	**16**	**63851836**	**IP10_S_typhimurium**	**3.70E-08**	**A**	**-**	**40.1%**	**9.1%**	**1.2%**
rs16956501	17	48419912	Chlamydia_70hr_median_GFP	1.10E-08	C	SKAP1	27.3%	22.6%	0.2%
rs4121804	18	59790252	Chlamydia_46hr_highGFP	4.11E-08	G	-	33.0%	20.1%	0.6%

*gene the SNP is located in or "near" (within 20kb)

885

STAR Methods

KEY RESOURCES TABLE

REAGENT or RESOURCE	SOURCE	IDENTIFIER
Antibodies		
Bacterial and Virus Strains		
S. enterica Typhi (strain Ty2) +pMMB67GFP	This paper	N/A
S. enterica Typhimurium (strain 14028s) +pMMB67GFP	Dennis Ko	(Ko et al., 2009)
S. enterica Typhimurium (strain 14028S *ΔsifA*) +pMMB67GFP	This paper	N/A
Chlamydia trachomatis LGV-L2, Rif^R + pGFP::SW2	Raphael Valdivia	(Bastidas and Valdivia, 2016)
Mucor circinelloides f. *lusitanicus* R7B (*leuA*-)	Soo Chan Lee	(Roncero, 1984)
Candida albicans SC5314	Joseph Heitman	(Odds et al., 2004)
Toxoplasma gondii strain RHgfpluc	John Boothroyd	(Saeij et al., 2005)
Biological Samples		
Chemicals, Peptides, and Recombinant Proteins		
alpha-hemolysin (Staph. aureus alpha toxin)	Sigma	H9395-.5MG
7-AAD	Enzo Life Sciences	BML-AP400-0001
Critical Commercial Assays		
Human FGF basic DuoSet	R&D Systems	DY233
Human IL-10 DuoSet	R&D Systems	DY217B
Human CXCL10 DuoSet	R&D Systems	DY266
Human MDC Duoset	R&D Systems	DY336
Human IL-6 Duoset	R&D Systems	DY206
Milliplex MAP Human Cytokine Custom 17-plex panel	Millipore EMD	HCYTOMAG

Deposited Data		
Illumina HumanOmni 2.5M array	1000 Genomes	ftp://ftp.1000genomes.ebi.ac.uk/vol1/ftp/release/20130502/supporting/hd_genotype_chip/
H2P2 database and web portal	This paper	h2p2.oit.duke.edu
Experimental Models: Cell Lines		
1000 Genomes LCLs	Coriell	GWD, ESN, IBD, KHV
Experimental Models: Organisms/Strains		
Oligonucleotides		
Accell siRNA for non-targeting #1, *ZBTB20*, *NFKBIA*	Dharmacon	D-001910-01-50; E-020529-00-0010; E-004765-00-0010
Taqman human gene expression assays for *ZBTB20*, *NFKBIA*, *18S RNA*,	ThermoFisher	Hs00210321_m1; Hs00355671_g1; Hs03928990_g1
Recombinant DNA		
Software and Algorithms		
PLINK v1.9	(Chang et al., 2015)	https://www.cog-genomics.org/plink/1.9/
LocusZoom	(Pruim et al., 2010)	http://locuszoom.sph.umich.edu/
IMPUTE v2.3.2	(Howie et al., 2009)	http://mathgen.stats.ox.ac.uk/impute/impute_v2.html
SHAPEIT v2.r790	(Delaneau et al., 2013)	https://mathgen.stats.ox.ac.uk/genetics_software/shapeit/shapeit.html

Samtools v1.5	(Li et al., 2009)	http://samtools.sourceforge.net/
GCTA v1.26	(Yang et al., 2011)	http://cnsgenomics.com/software/gcta
GARFIELD	(Iotchkova et al., 2016)	http://www.ebi.ac.uk/birney-srv/GARFIELD
CIRCOS v0.69	(Krzywinski et al. 2009)	http://circos.ca/software/download/circos/
ANNOVAR v2016FEB01	(Wang et al., 2010)	http://annovar.openbioinformatics.org/
GGV Browser	(Marcus and Novembre, 2017)	http://popgen.uchicago.edu/ggv/
Phenogram	(Wolfe et al., 2013)	http://visualization.ritchielab.psu.edu/phenograms/plot
R v3.3.2	(Team, 2016)	https://cran.r-project.org/
ggplot2	The R Foundation	https://cran.r-project.org/web/packages/ggplot2/index.html
data.table	The R Foundation	https://cran.r-project.org/web/packages/data.table/index.html
dplyr	The R Foundation	https://cran.r-project.org/web/packages/dplyr/index.html
biomaRt	Bioconductor	https://bioconductor.org/packages/release/bioc/html/biomaRt.html
stringr	The R Foundation	https://cran.r-project.org/web/packages/stringr/index.html
RColorBrewer	The R Foundation	https://cran.r-project.org/web/packages/RColorBrewer/index.html
reshape2	The R Foundation	https://cran.r-project.org/web/packages/reshape2/index.html

GenomicRanges	Bioconductor	https://bioconductor.org/packages/release/bioc/html/GenomicRanges.html
PheWAS	The R Foundation	https://phewascatalog.org/
Other		

CONTACT FOR REAGENT AND RESOURCE SHARING

Further information and requests for reagents should be directed to and will be fulfilled by the Lead Contact, Dennis Ko (dennis.ko@duke.edu).

EXPERIMENTAL MODEL AND SUBJECT DETAILS

Cells

1000 Genomes LCLs (528; all trios) from ESN (Esan in Nigeria), GWD (Gambians in Western Divisions in the Gambia), IBS (Iberian Population in Spain), and KHV (Kinh in Ho Chi Minh City, Vietnam) populations were purchased from the Coriell Institute. LCLs were maintained at 37˚C in a 5% CO_2 atmosphere and were grown in RPMI 1640 media (Invitrogen) supplemented with 10% fetal bovine serum (FBS), 2 mM glutamine, 100 U/ml penicillin-G, and 100 mg/ml streptomycin.

METHOD DETAILS

LCL screening

LCLs were received from Coriell and cultured for 8 days prior to assays. LCLs were counted with a Guava Easycyte Plus flow cytometer (Millipore). LCLs were washed once with RPMI 1% FBS and then plated out in RPMI 10% FBS at 200,000 cells/200µl for Salmonellae, 100,000 cells/100µl for fungi, and 40,000 cells/100µl for *S. aureus* alpha toxin, *C. trachomatis,* and *T. gondii*. Cells were passaged at 150,000/ml in 20ml total volume for three days.

C. trachomatis infection

C. trachomatis LGV-L2 Rif^R pGFP::SW2 was grown and purified as previously described (Saka et al., 2011). *C. trachomatis* was added at MOI 5 in 100µl assay media, mixed by multichannel pipetting, and centrifuged onto cells at 3000 RPM for 30min at 4ºC. At 27, 46, and 70hrs, cells were mixed and 25ul of cells were taken for flow cytometry measurement (4000 cells). 25 ul of supernatant at 70hrs was measured by Luminex assay for 17 cytokines.

Salmonella infection

Salmonellae were tagged with an inducible GFP plasmid [pMMB67GFP from (Pujol and Bliska, 2003)]. *sifA* deletion mutants was constructed with lambda red (Datsenko and Wanner, 2000) and verified by PCR. Assaying LCLs for Salmonellae infection was conducted as previously described (Ko et al., 2009). Overnight bacterial cultures were subcultured with a 1:33 dilution and grown for 2 hr 40 min at 37˚C. Invasion was conducted for 1hr at a multiplicity of infection (MOI) of 10 for *S.* Typhi and MOI 30, followed by addition of gentamicin (50ug/ml) for 1hr, and then culture was split into two separate cultures of 60ul of cells with 140ul of media to dilute gentamicin (15ug/ml) and allow for collection at two timepoints. IPTG (1.4mM) was added to turn on GFP expression for 75 min prior to 3.5hr and 24hr timepoints. For the 3.5hr timepoint, 150ul of cells were stained with 7-AAD (7-aminoactinomycin D; Enzo Life Sciences) and green and red fluorescence of 7000 cells was measured on a Guava Easycyte Plus flow cytometer

(Millipore). For the 24hr timepoint, cells were spun down and 2 aliquots of 55ul of supernatant was removed and stored at -80C for subsequence IL10 (25ul), CXCL10 (25ul), and MDC (4ul) ELISAs (R&D Systems). 55ul of cells were stained with 7-AAD and measured by flow cytometry.

Fungal infection

The *Mucor circinelloides* f. *lusitanicus* R7B (*leuA*-) (Roncero, 1984) strain and *Candida albicans* SC5314 (Odds et al., 2004) strain were used as wild-type to test the expression of FGF-2 from the LCLs. Leucine autotropism (*leuA*$^{-}$) was found not to impact virulence (Li et al., 2011). To prepare *Mucor* spores, potato dextrose agar (PDA, 4 g potato starch, 20g dextrose, and 15 g agar per liter) was inoculated and incubated for 4 days at 26°C in the light. To collect spores, sterile deionized distilled water was added onto the plates and spores were released by gently scraping the colonies with a cell spreader. Spores were counted by using a hemocytometer. To prepare *C. albicans* yeast, yeast dextrose broth (10 g yeast extract, 20 g peptone, 20 g glucose per liter) was inoculated and incubated at 30°C by shaking at 250 rpm overnight. The yeast cells were quantified by using a hemocytometer. To co-culture with LCLs, all fungal cells were washed with sterile PBS twice. Fungi were added at MOI 1 in 10 µl and incubated for 24 hrs. Culture supernatant was collected and stored at -80°C for later FGF-2 ELISA analysis (R&D Systems).

***S. aureus* toxin treatment**

LCLs were treated with alpha-hemolysin (Sigma) at 1µg/ml for 23hrs. Cells were mixed and cell death quantified by 7-AAD staining (concentration) and flow cytometry.

***T. gondii* infection**

T. gondii strain RHgfpluc was grown on confluent human foreskin fibroblast cells. The infected cells were then scraped and transferred to a 50ml polystyrene tube and centrifuged at 500 x g for 10 minutes at 4°C. Pellet was resuspended in 3 ml of PBS and the suspension was aspirated three times using a 20g needle attached to a 10ml syringe. 30 ml of PBS was added and centrifuged at 500 x g for 10 min at 4°C. Supernatant was removed, and pellet resuspended in 5ml of PBS. Concentration of a 1:200 dilution was determined by flow cytometry and added at MOI 2 to cells. At 5, 30, and 48 hrs infection, cells were mixed, and 25ul taken for measuring 4000 cells by flow cytometry.

RNAi experiments

LCLs ($2x10^5$ cells) were treated for three days in 500µl of Accell media (Dharmacon) with either non-targeting Accell siRNA #1 or an Accell SmartPool directed against human *ZBTB20* or *NFKBIA* (1µM total siRNA; Dharmacon). Prior to infection, cells were plated at $1x10^5$ in 100µl RPMI complete media (without antibiotics) in 96-well plates. Infections were conducted as described above.

Literature search

To determine if SNPs in CXCL10 had previously been associated with infections disease, we performed a PubMed search on May 1, 2017 using the query "CXCL10 polymorphisms." The search revealed 92 publications and each was examined individually for *CXCL10* SNPs that had been tested for an association with infectious disease. Several studies examined rs56061981 but this SNP is not in LD with rs2869462 (r^2=0.01 in Europeans) and shows no association with CXCL10 levels in our dataset (p=0.90). In contrast, rs3921 is in LD with rs2860462 (r^2=0.3 in Europeans) and is associated with CXCL10 levels ($p=6.4x10^{-4}$). Five publications had examined the association of rs3921 and infectious disease (Fisher et al., 2017; Mezger et al., 2008;

Nogueira et al., 2012; Pineda-Tenor et al., 2015; Pineda-Tenor et al., 2014). Odds ratios and p-values reported in these studies were plotted in a forest plot (Figure 6A). As the CXCL10 gene is encoded by the minus strand and the two alleles are C and G, we verified the direction of effect based on the minor allele and the number of individuals reported of each genotype.

QUANTIFICATION AND STATISTICAL ANALYSIS

Phenotype repeatability

Repeatability of each cellular trait was calculated to measure the variation among 3 independent experiments. The inter- and within-individual component of variance was calculated by fitting to one-way ANOVA. The estimated within-individual component of variance gave the repeatability coefficient.

Genotype and imputation

Genotypes for 1000 Genome LCLs (Consortium, 2010) were from Illumina HumanOmni 2.5M array (905,788 SNPs; see details in STAR resource table). Genome-wide imputation of autosomal genotypes with 1000 genome Phase 3 haplotype as reference panel were performed through two steps, a pre-phasing step using SHAPEIT2 (Delaneau et al., 2013) and an imputation step using IMPUTE2 (Howie et al., 2012). Imputed genotype was further filtered by imputation accuracy score (IMPUTE's INFO) < 0.9 and minor allele frequency < 0.01. A total of 339 samples overlap with 1000 genome Phase 3 individuals. We merged those direct sequenced genotypes from 1000 genome Phase 3 project into our imputed genotypes. We eventually obtained 15,581,278 SNPs (8,817,925 SNPs have minor allele frequency ≥ 0.05). The human genome reference assemble (GRCH37/hg19) was used for all analysis.

Phenotype- and SNP-based heritability analysis

Two different methods were applied to estimate heritability. The parent-offspring (PO) regression method estimated additive heritability exclusively using phenotypic values. Linear regression of child against average of parents was performed, and the slope was used as a heritability estimator. Batch was incorporated as a covariate. Genotype-based heritability was estimated using the GCTA GREML method (Yang et al. 2012). Autosomal SNPs with minor allele frequency filtering of 0.05 were used to create a genetic relationship matrix (GRM). Zaitlen and colleagues developed a method, "big K/small K", which enables to precise estimate heritability by jointly using closely related and unrelated individuals (Zaitlen et al., 2013). Following Zaitlen's method, variance explained by genome-wide SNPs (σ_g^2) was then estimated for each cellular trait. The Zaitlen modification provides joint estimates of 1) h^2 based on pedigree relatedness and 2) h^2 based on inferred relatedness from genome-wide SNPs.

While the standard error for SNP-based h^2 estimates were quite large, we nonetheless observed very strong correlation between these estimates and the parent-offspring h^2 estimates (see Figure 1D). We estimated h^2 based on the analysis of LCLs from all populations in H2P2 to increase the precision of our estimates by including more individuals. Although h^2 is a population-specific parameter, h^2 are often quite similar across different populations and even species (Visscher et al., 2008). Nonetheless, we include estimates and standard errors for the combined analysis as well as individual populations in Table S2.

Genome-wide association analysis

Genome-wide association analysis was conducted with PLINK v1.9 (Purcell et al., 2007). Analysis was carried out using the QFAM-parents approach with adaptive permutation and maximum of 10^9 permutations. The QFAM procedures implemented in PLINK use linear

regression to test for association while employing permutation of within- and between-family components separately to control for family structure (Purcell et al., 2005).

Enrichment analysis

Enrichment analyses were carried out using GARFIELD (Iotchkova et al., 2016). GARFIELD has predefined a total of 1005 features from ENCODE and the NIH Roadmap project, and applies generalized linear regression models while accounting for the effects of linkage disequilibrium (LD), minor allele frequency, and local gene density. The GWAS summary statistics were used to quantify fold-enrichment against predefined annotation features at different GWAS p-value thresholds.

PheWAS Analysis

Testing for association of H2P2 genome-wide hits with clinical phenotypes was performed with the eMERGE biobank dataset of 83,717 individuals from 12 contributing medical centers (Crosslin et al., 2014; Gottesman et al., 2013; McCarty et al., 2011; McDavid et al., 2013) with ICD-9 derived PheWAS codes (Carroll et al., 2014; Denny et al., 2013). A merged set of unified variant genotypes across 78 batches of samples with different genotype platforms (e.g. various Illumina and Affymetrix arrays) was produced by imputation using the Michigan Imputation Server (MIS) with the HRC1.1 haplotype reference set (Das et al., 2016; Loh et al., 2016; McCarthy et al., 2016). Sixteen variants were selected for PheWAS based on association in H2P2 and their inclusion in the imputed eMERGE biobank dataset. The PheWAS codes were defined by query of the ICD-9 electronic medical record datasets of the contributing medical centers. Two types of PheWAS code phenotypes were used in the association to ascertain more chronic versus singleton diagnoses. The minimum code count of one (mcc1) ICD-9 code to define an individual as a PheWAS code case, and minimum code count of two (mcc2) instances

to define and individual as a chronically represented case. In the mcc2 cases, individuals were excluded from analysis if they only had one instance of the ICD-9 code. If there were less than 100 cases we did not include the ICD-9 derived PheWAS code in analysis because it would likely be underpowered and impact the multiple testing correction. This resulted in 1387 phenotypes being included in the analysis. We used the software PRIMUS (Staples et al., 2013; Staples et al., 2014) on the PLINK1.9 identity by descent genome file to find the maximal set of unrelated individuals to bring forward for analysis. PheWAS association and plotting was carried out using the PheWAS R package (Carroll et al., 2014) which uses the R glm() logistic regression model for case-control data. The covariates of gender and the PLINK1.9 computed 1 to 10 principal components from the pruned (>5% minor allele frequency, genotype and sample missingness > 0.1 and LD r-square<0.7.) genome wide imputation variant genotypes were included in the regressions. The p.adjust() R function with the FDR method was used to adjust p-values of the tested PheWAS codes within a particular SNVs sets of tests for multiple comparisons. The FDR of less than 0.3 was used as a significance threshold.

Descriptive statistics and visualization

Descriptive statistics were performed with GraphPad Prism 6 (GraphPad Software, US) and with R (Team, 2016). QQ plots were plotted using quantile-quantile function in R. Regional Manhattan plot were made using LocusZoom (Pruim et al., 2010). Circos v0.69 was used to visualize the shared SNPs among different groups.

The size of each study or number of replicates, along with the statistical tests performed can be found in Figure Legends. All numerical data are presented as the mean ± SEM (standard error of mean).

DATA AND SOFTWARE AVAILABILITY

All H2P2 data is available for browsing and download at http://h2p2.oit.duke.edu

The H2P2 application server is running Red Hat Enterprise Linux Server v7.4, Apache v2.4.6, Shiny Server v1.5.3.838, R v3.4.1, and Microsoft ODBC Driver 13 for SQL Server. Implemented R packages include shiny v1.0.3, RODBC v1.3-15, ggplot2 v2.2.1, d3heatmap v0.6.11, and DT v0.2. The H2P2 database server is running MS Windows Server 2016 and MS SQL Server 2016. Large volume tables and indexes (2.5 billion GWAS observations and 8.5 billion genotype observations) were partitioned for improved query performance. Parallelized query implementation was also used to improve performance.

Supplemental Information

Table S1. Phenotype definitions and representative flow cytometry plots.

Figure S1. Histograms of 79 H2P2 traits. For flow cytometric data, raw phenotype values are used. For cytokine data, concentrations are log2 transformed.

Figure S2. Repeatability of 79 H2P2 traits. Repeatability was calculated as the inter-individual component of variance from ANOVA of 3 measurements of LCLs taken on sequential cell passages. Phenotypes are color-coded by stimuli. All traits have significant repeatability ($p<0.05$ marked by asterisk), except for three of the toxoplasma traits.

Figure S3. Heritability of 79 H2P2 traits by parent-offspring regression. Individual plots for all H2P2 traits are shown with parent-offspring regression lines with (blue) and without (red) batch covariate. Estimated h^2 and p-value for parent-offspring regression with batch covariate are listed on each plot.

Table S2. Heritability of 79 H2P2 traits by parent-offspring regression and SNP-based heritability.

Figure S4. QQ plots of 79 H2P2 traits. All SNPs with MAF > 5% are shown.

Table S3. eMERGE PheWAS results for 16 H2P2 hits. All eMERGE phenotypes with FDR < 0.3 are shown.